Large-Scale Common Features of Subtropical Precipitation Zones (the Baiu Frontal Zone, the SPCZ, and the SACZ) Part I: Characteristics of Subtropical Frontal Zones

By Yasumasa Kodama

Department of Earth Science, Faculty of Science, Hirosaki University, Hirosaki 036, Japan
(Manuscript received 7 October 1991, in revised form 26 May 1992)

Abstract

In East Asia, a quasi-stationary frontal zone called the Baiu frontal zone (BFZ) forms during the early summer and provides nearly as much precipitation as the Intertropical Convergence Zone (ITCZ). Since the BFZ has several characteristics different from both the ITCZ and polar frontal zones, Ninomiya (1984) proposed the BFZ should be classified as a subtropical frontal zone.

Using mainly ten-day mean data, we compare the BFZ around Japan with the subtropical portions of the South Pacific Convergence Zone (SPCZ) and the South Atlantic Convergence Zone (SACZ), which are significant precipitation zones in the summer Southern Hemisphere. These three precipitation zones are shown to have several common features as the following.

The BFZ, the SPCZ, and the SACZ (hereafter referred to as the SPZs, the Subtropical Precipitation Zones) commonly form along the subtropical jet on the eastern side of a quasi-anchored trough, which lies to the northeast (in the Northern Hemisphere) or southeast (in the Southern Hemisphere) of the localized active convection of the tropical monsoon. The rainfall amount in the SPZs attains ~400 mm/month when they are active. All of the SPZs are characterized by convergence zones with an interior thick moist layer and baroclinic zones with an upper subtropical jet. They are also characterized as poleward boundaries of the moist tropical or monsoon airmass associated with a low-level large gradient of moisture mixing ratio.

Since the evaporation rate is much smaller than the precipitation rate along the SPZs, high rainfall in the SPZs is maintained by the convergence of two types of moisture currents in the SPZs. One is eastward along the SPZ and the other is along the northwestern (in the N.H.) or the southwestern (in the S.H.) periphery of the subtropical high. The latter transports moisture evaporated under the western part of the subtropical high. Generation of convective instability by the differential advection process is found along the SPZs and maintains active convection along the SPZs.

Since the SPCZ and the SACZ have several unique characteristics different from the ITCZ and polar frontal zones but similar to the BFZ, it is concluded that all of the SPZs can be classified as subtropical frontal zones.

1. Introduction

Precipitation is one of the meteorological elements which strongly influence agricultural productivity. Recently, many people have become interested in climatic changes in global rainfall distribution which may occur in association with the increase of CO_2. To predict these changes, we must understand the mechanisms determining the present rainfall distribution.

In the global rainfall distribution, the tropics, where monsoon convections and the ITCZ develop, and the mid-latitudes, where the polar frontal zones (PFZs) form, are two major precipitation zones, while the subtropics lying between them are characterized as dry zones. In the East Asia subtropics, however, a quasi-stationary precipitation zone referred to as the Baiu frontal zone (BFZ) appears during the early summer between May and July and provides rainfall up to ~400 mm/month, which is comparable to that of the ITCZ. Although the rainfall amount in the subtropics generally increases during the summer on the east coast of continents (Trewartha, 1968). the amount is much larger in East Asia, where the Baiu front stagnates, than in other east coastal areas in the subtropics.

In the East Asia subtropics, a distinct frontal zone with much cloudiness appears throughout the year except in August (*e.g.*, Yoshimura, 1967; Nitta,

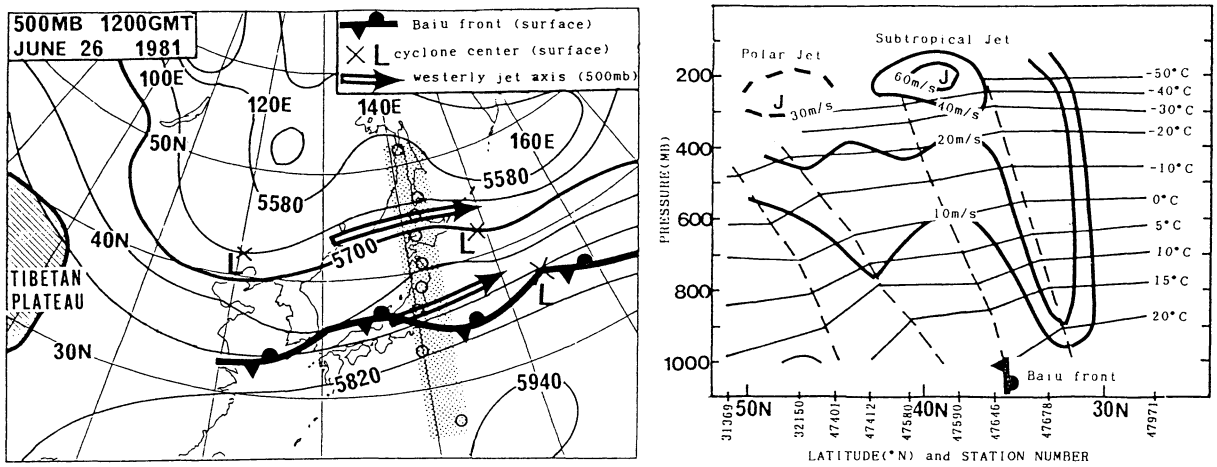

Fig. 1. An example of circulation around the Baiu front. Left panel shows height fields (the contour interval is 60 m) and jet axes at 500 mb and the positions of the Baiu front and cyclone center at the surface. Right panel shows a cross-section of temperature and wind speed. Stipple and open circles in the left panel show the positions of the cross-section and aerological observation stations, respectively.

1986; Kodama and Asai, 1988). The BFZ, characterized by its quasi-stationarity, appears in early May around 25°N between the eastern foot of the Tibetan Plateau and the central North Pacific (*e.g.*, Kato and Kodama, 1992). The zone shifts northward gradually with the seasonal march and disappears around 40°N in late July (Yoshino, 1966).

The BFZ changes its characteristics twice with the seasonal march: once around late May when the low-level temperature gradient of the BFZ almost disappears over the China Continent owing to strong heating with a hot land-surface to the north of the zone (Kato, 1985, 1987); again when the low-level moist southerly to the BFZ is intensified along the western periphery of the subtropical high in middle June (Kato, 1989). After the latter change, the rainfall amount of the BFZ increases (Yoshino, 1966) and the BFZ is considered to attain its peak period (Ninomiya and Muraki, 1986) before its disappearance in late July. In this study, we will investigate the BFZ during its peak period.

In the peak period of the BFZ, a quasi-anchored trough appears to the west of Japan (Saito, 1985) and the upper westerlies split into a subtropical jet and a polar jet over Japan (Murakami, 1951). Except over the continent, the BFZ appears along the subtropical jet in the eastern part of the trough. An example of the circulation around the Baiu front is shown in Fig. 1 with a latitude-height cross-section of temperature and wind speed. The Baiu front at the surface is associated with a temperature gradient subsiding from the upper subtropical jet.

Many observational studies pointed out several large-scale unique characteristics of the BFZ during the peak period (*e.g.*, Murakami, 1959; Saito, 1966; Kurashima and Hiranuma, 1970; Ninomiya, 1984; Ninomiya and Muraki, 1986). Furthermore, Akiyama (1978) pointed out that the Baiu front has a unique meso-α-scale precipitation system composed of stratiform and convective echo areas, which appear in the northern and southern parts of the system, respectively.

Ninomiya (1984) compared the BFZ to other PFZs in the summer Northern Hemisphere (N.H.) and summarized the large-scale characteristics of the BFZ which are different from the PFZs as follows; a steady precipitation zone with a strong gradient of equivalent potential temperature and moisture mixing ratio, an interior thick moist layer, the generation of convective instability, large moisture flux convergence, and significant upward motion. From these features, he proposed that the BFZ is not a PFZ but a significant subtropical frontal zone in East Asia and that no other similar frontal zones are observed in the summer N.H.[1]

The reasons why such a unique frontal zone appears only over East Asia and the western North Pacific have interested many meteorologists. Many observational and numerical studies have suggested that the Tibetan Plateau, Asian summer monsoon, and the subtropical high over the western North Pacific strongly influence the formation of the BFZ (*e.g.*, Murakami, 1956; Asakura, 1970; Akiyama, 1973; Nakamura and Hasegawa, 1987; Kato, 1989). However, we cannot explain the mechanisms for the

[1]There has been a controversy over the classification of the BFZ. In the 1940s, meteorologists in China thought the BFZ is a tropical frontal zone (Kurashima, 1959), while, Kurashima and Hiranuma (1970) thought that the BFZ should be classified as a tropical frontal zone over the China continent and as a polar frontal zone to the east of Japan. In this study, the portion of the BFZ around Japan is classified as a subtropical frontal zone, because the characteristics of the BFZ as a subtropical frontal zone are most clearly observed around Japan (Ninomiya, 1984).

formation of the BFZ satisfactorily yet.

According to the studies of the climatic frontal zones in summer, there is a group of frontal zones which appear in the lower latitudes at 30°–40° besides the group of circumpolar frontal zones in the higher latitudes at 50°–70° (*e.g.*, Yoshimura, 1967; Taljaard, 1968). In the summer N.H., the BFZ and the frontal zone along the east coast of North America belong to the group of the lower-latitude zones. A front, however, appears much more frequently in the subtropics at ~30°N in the BFZ than in the zone along the east coast of North America (cf., Fig. 3 of Yoshimura (1967)), and only the BFZ has the characteristics of a subtropical frontal zone (Ninomiya, 1984). In the summer Southern Hemisphere (S.H.), on the other hand, two frontal zones appearing in the subtropics at ~30°S over the central South Pacific and the western South Atlantic (cf., Fig. 5 of Taljaard (1968)) belong to the group of the lower-latitude zones, although it has not been clarified yet whether these zones have the characteristics of subtropical frontal zones.

In satellite cloud images, these frontal zones in the S.H. are observed as subtropical portions of quasi-stationary significant cloud zones which extend between the tropics and the extra-tropics (Streten, 1973; Yasunari, 1977). Since the cloud zones have the characteristics of convergence zones, the zones over the central South Pacific and over the South Atlantic are referred to as the South Pacific Convergence Zone (SPCZ) and the South Atlantic Convergence Zone (SACZ), respectively. The characteristics of these zones vary with latitude. Trenberth (1976) suggested that the tropical portion of the SPCZ in characterized by a convergence zone similar to the ITCZ and the subtropical and extra-tropical portions of the SPCZ are characterized as both convergence zones and frontal zones.

The subtropical portions of the SPCZ and the SACZ are, thus, likely to have characteristics different from both typical PFZs and the ITCZ. Furthermore, several studies of the SPCZ suggested that the subtropical portion of the SPCZ has unique characteristics which may be similar to those of the BFZ, *e.g.*, its quasi-stationarity continuing for about ten days (Vincent, 1982; Huang and Vincent, 1983) and its meso-α-scale frontal depressions (Vincent, 1985).

Thus, it is desirable to clarify whether the SPCZ and the SACZ are Southern Hemisphere versions of the BFZ. We think that such a comparative study is useful for understanding the relationship between the BFZ and its surroundings (*e.g.*, Tibetan Plateau, land-ocean distribution, summer monsoon, and the subtropical high over the western North Pacific) which have been stressed to be important in forming the BFZ, because the surroundings of the three frontal zones are different from one another. Unfortunately, such a comparative study has not been done, except for several suggestions by Murakami (1986) and Ogawa (1982) regarding their similarities.

In the present study, we will confine our attention to the large-scale characteristics of the BFZ compared with those of the SPCZ and the SACZ using mainly ten-day mean objective analysis data. In Part I of the study, the similarities of subtropical frontal zones, which are different from both the PFZs and the ITCZ, will be discussed. In Part II, the similarities observed in the relationship between the frontal zones and monsoon circulations will be discussed.

The BFZ, the SPCZ, and the SACZ change their characteristics spatially and seasonally. We confine, therefore, the study areas and periods. For the BFZ, its portion around Japan between 120°E and 160°E for the period from June to July, nearly corresponding to the peak period of the BFZ, is studied. This is because the BFZ over the continent is largely aeffected by strong land surface heating (Kato, 1985) and the characteristics of the BFZ as a subtropical frontal zone are obscure to the east of Japan (Ninomiya, 1984). For the SPCZ and the SACZ, only their subtropical portions between 25°S and 40°S are studied, because their characteristics largely vary with latitude (*e.g.*, Trenberth, 1976; Vincent, 1982). Study periods for the SPCZ and the SACZ are southern summer between December and March, in accordance with the definition of the seasons in the S.H. by Taljaard (1967).

Since the three frontal zones (the BFZ, the SPCZ, and the SACZ) produce much rainfall, as shown in Senction 4, we will refer to their subtropical portions as the Subtropical Precipitation Zones (the SPZs).

2. Data

To investigate the large-scale characteristics of the SPZs, we utilized twice-daily global objective analysis data for 1981, 1982, 1983, and 1985. For the reasons associated with data acquisition, 1984 was excluded. Origins of the data are NMC (National Meteorological Center, U.S.A.) for 1981, 1982, and 1983 and JMA (Japan Meteorological Agency) for 1985. Grid-spacing of the data is 2.5° in both longitude and latitude. Satellite cloud winds and vertical temperature sounding data were utilized for the objective analysis of these data. For a further explanation of the objective analysis refer to McPherson *et al.* (1979) and Dey and Morone (1985) for the NMC data and to Kanamitsu *et al.* (1983) for the JMA data.

In these data, we utilized geopotential height, temperature, and wind at 8 levels of 100 mb, 200 mb, 300 mb, 400 mb, 500 mb, 700 mb, 850 mb, and 1000 mb (NMC) or surface (JMA), and utilized relative humidity (NMC) or dew point temperature (JMA) at the same levels below the 400 mb level.

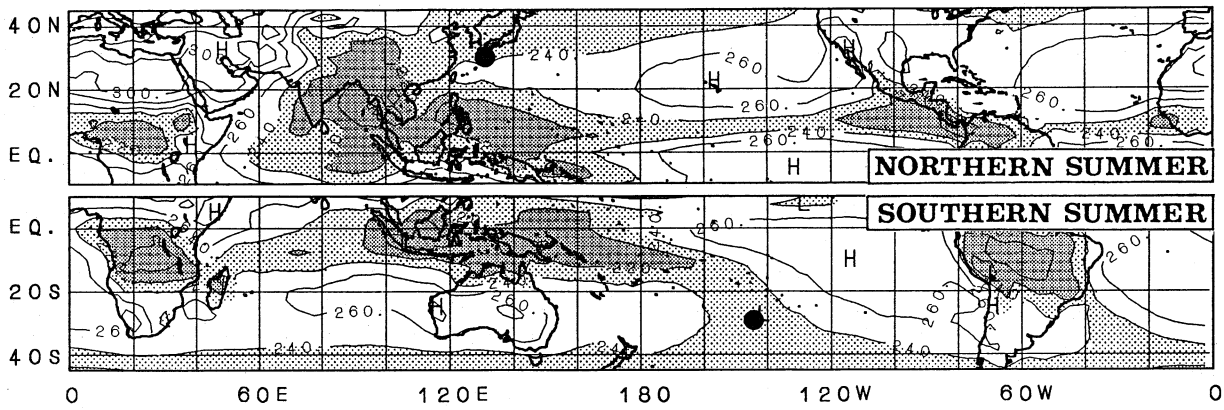

Fig. 2. OLR fields in the Northern Hemisphere summer (from June to August; upper panel) and in the Southern Hemisphere summer (from December to February; lower panel) averaged for the eight years from 1979 to 1986. Contour interval is 20 W/m^2. The areas of OLR between 240 W/m^2 and 220 W/m^2 are thin shaded and less than 220 W/m^2 are thick shaded. Black circles indicate the positions of observation stations, Kagoshima (31°N, 130°E) and Rapa (28°S, 144°W).

To discuss the configuration and rainfall activities of the SPZs, we utilized twice-daily OLR (Outgoing Longwave Radiation) data (Winston and Krueger, 1977) for the eight years from 1979 to 1986, because the OLR is useful for investigating large-scale distributions of cloudiness and convective activities. Furthermore, we utilized station data of precipitation to investigate the rainfall amount over the SPZs. Sources of the station data will be shown later.

3. Configurations

Figure 2 shows OLR fields during the summer averaged for the eight years from 1979 to 1986. The upper panel is for the N.H. summer (June–August) and the lower is for the S.H. summer (December–February). Here, we confine our attention to the subtropics defined as the zone between 25 and 40 latitude of each hemisphere.

In the summer N.H., only the BFZ has a significant cloud band, which extends from East Asia to the North Pacific with low OLR less than 240 W/m^2. We can find another low OLR area over the western North Atlantic along the east coast of North America. Its OLR value in the subtropics is, however, much larger than that of the BFZ, which suggests its rainfall activity is much weaker than the BFZ.

In the summer S.H., two significant cloud bands are found over the central South Pacific and the South Atlantic, which correspond to the SPCZ and the SACZ, respectively. They extend between the tropics and the extra-tropics with northwest-southeast tilted structures. Their OLR is less than 240 W/m^2, as low as that of the BFZ. Although another low OLR area is found over the western Indian Ocean around the east coast of Africa in the S.H., its OLR is much larger than those of the SPCZ and the SACZ, and its rainfall activity seems to be weak.

As shown above, only the BFZ, the SPCZ, and the SACZ are significant subtropical precipitation zones during the summer. Land-sea distributions surrounding the SPZs are different from one another. It should be remarked that the three SPZs commonly extend eastward to the subtropics from localized active convection in the tropics which are shown by low OLR of less than 220 W/m^2, although the BFZ is oriented more zonally than the SPZs in the S.H. Furthermore, other weak cloud bands around the east coast of North America and Africa in the S.H. also extend from localized convection in the tropics. These features strongly suggest that localized convection largely contributes to the formation of precipitation zones in the subtropics.

Murakami and Nakazawa (1985) referred to the localized active convection in the tropics observed around the three continental areas (Asia, Africa, and North and South America) as monsoons, because seasonal migrations of the convection are significant. Since the localized convection in the tropics, from which the SPZs extend, seem to agree with the monsoons referenced by Murakami and Nakazawa (1985), the localized active convection will be referred to as the monsoon convection in this study.

The SPZs vary significantly with an intraseasonal time-scale of around 30–60 days, although the period is determined not from quantitative analysis but from qualitative observations of cloudiness fields. Figure 3 shows an example of the intraseasonal variation of the SPCZ using ten-day mean high-cloudiness fields over the South Pacific between January and March in 1979 together with mean daily rainfall amount observed at Rapa (28°S and 144°W, shown by black circles in Fig. 3). The source of the rainfall data is the FGGE (the First GARP Global Experiment) level II-c precipitation and snow data set. In this study, the high-cloudiness is defined as the amount of cloud with tops higher

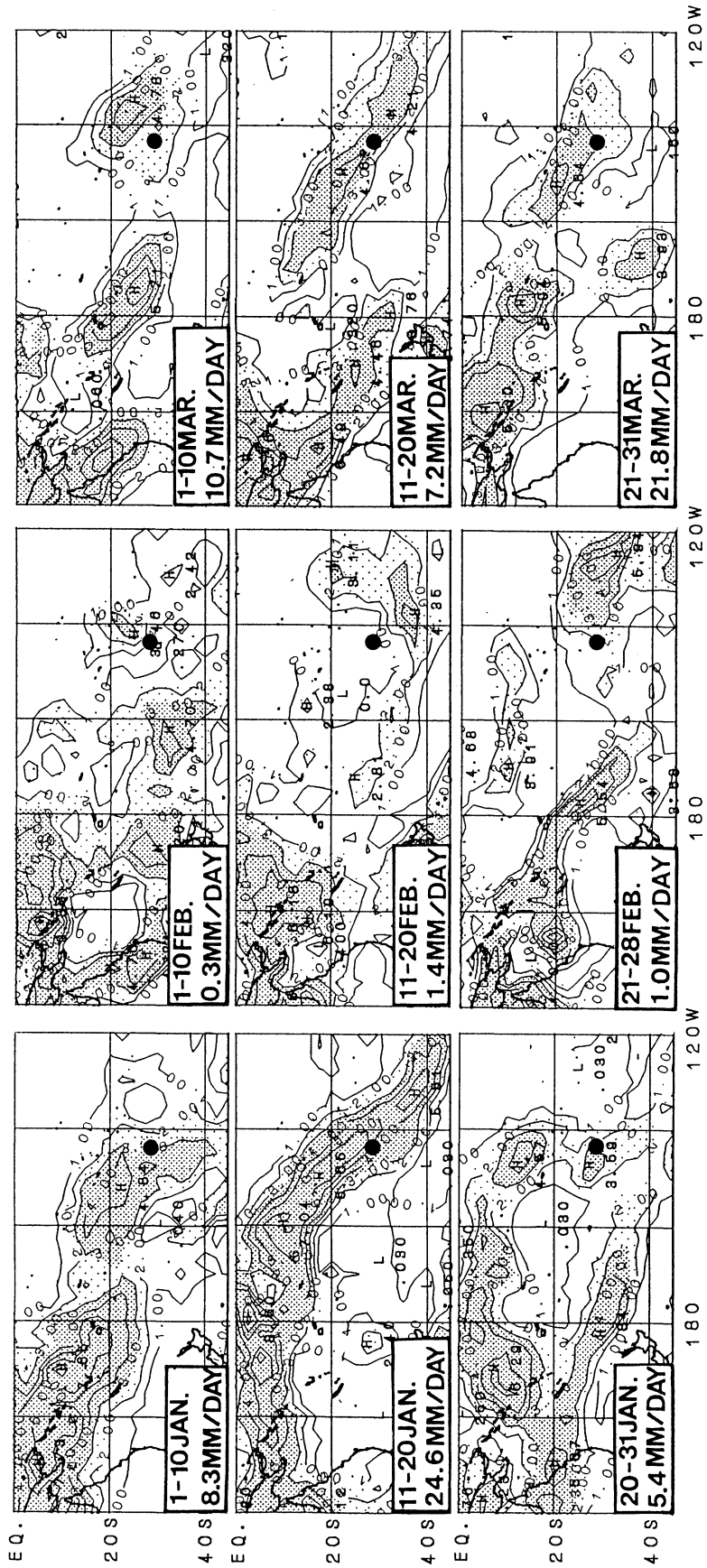

Fig. 3. High-cloudiness fields during nine ten-day periods from January to March in 1979 and mean daily amount of rainfall observed at Rapa in each period. The contour interval is 1/10; the areas the high-cloudiness between 2/10 and 3/10 are thin shaded and more than 3/10 are thick shaded. Black circles indicate the position of Rapa (28°S, 144°W).

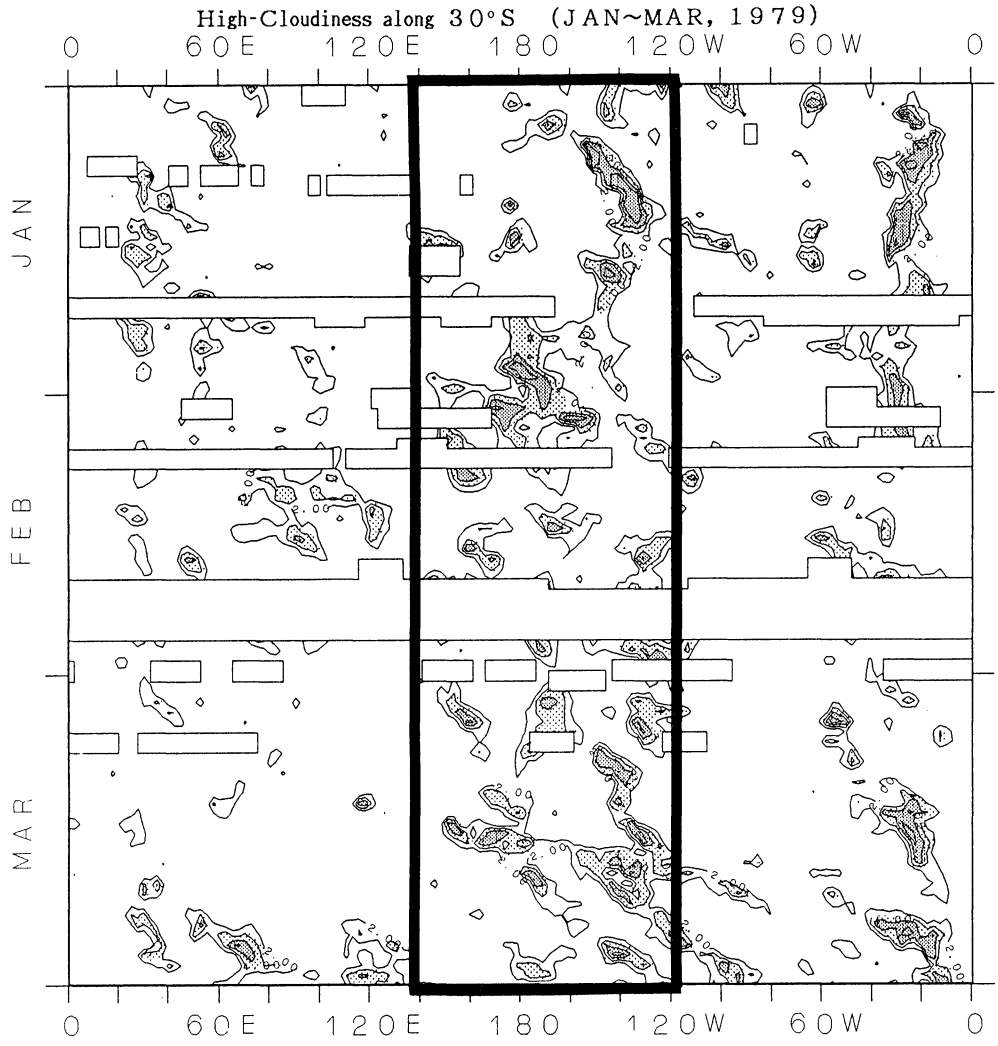

Fig. 4. Daily variations of high-cloudiness along 30°S between January and March, 1979. The contour interval is 2/10; the areas of high-cloudiness between 4/10 and 6/10 are thin shaded and more than 6/10 are thick shaded. Missing data are linearly interpolated. However, the periods when the missing data continue for more than two days are indicated as white areas framed in thin lines in place of the high-cloudiness. A frame of thick lines indicates the western and central Pacific area shown in Fig. 3.

than the 400 mb level and derived from the OLR based on statistical relationships between the daily mean values of the OLR and the high-cloudiness. A more detailed explanation of the transformation in given in the Appendix.

To interpret the variations of the SPCZ observed in the ten-day mean fields, daily variation of the high-cloudiness along 30°S is shown in Fig. 4. Missing data of the OLR were linearly interpolated before calculating the high-cloudiness, though the cloudiness was not shown in Fig. 4 when missing data continued for more than two days.

As shown in Fig. 3, the SPCZ does not always show a clear band-like structure. At times it almost disappears and sometimes becomes several weak cloud bands oriented in parallel. These intraseasonal variations of the SPCZ substantially affect the precipitation observed at Rapa.

During the first and second ten days in January, the SPCZ stagnated around 140°W (Fig. 4) and appeared as a clear cloud bands in the ten-day mean fields (Fig. 3). From the last ten days in January to the first ten days in March, the SPCZ was disrupted or weakened (Fig. 4) and lost its band-like structure in the mean fields (Fig. 3). After the second ten days in March, the SPCZ recovered its band-like structure (Fig. 3) and stagnated around 140°W, although it was associated with short-period eastward movement (Fig. 4). In Fig. 4, the intraseasonal variation of the SACZ is also shown. The SACZ stagnated around 20°W with much cloudiness before the first ten days February. It weekened between te second ten days in February and the first ten days in March, and became migratory around 20°W after the second ten days in March.

As shown above, day-to-day variations of the

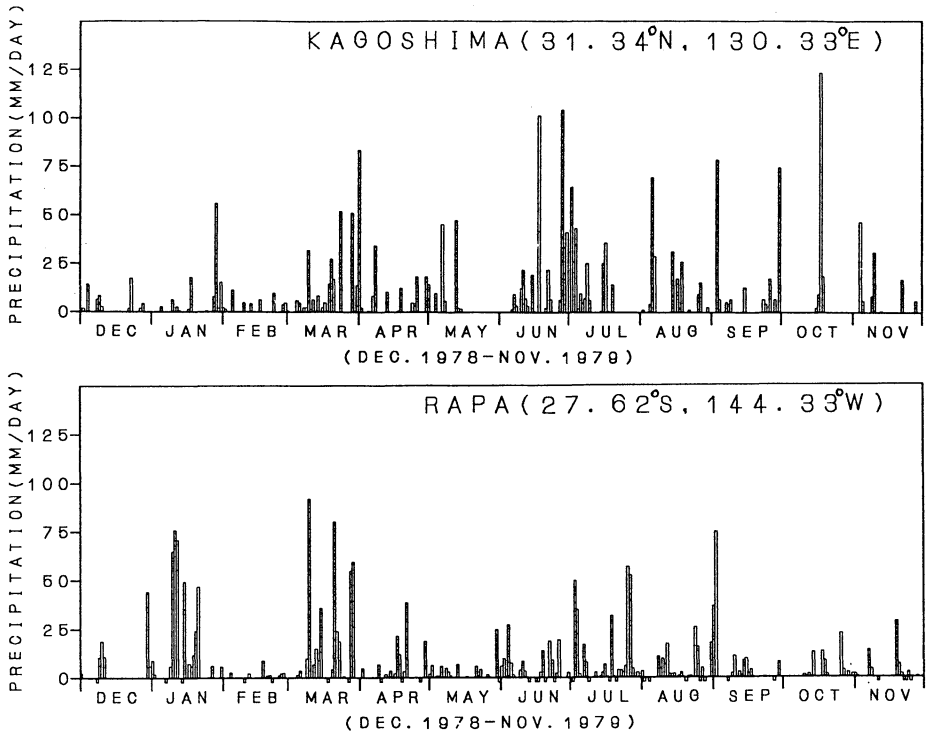

Fig. 5. Daily variations of rainfall amount observed at Kagoshima (upper panel) and Rapa (lower panel) during the FGGE year from December 1978 to November 1979. Minus bars at Rapa indicate the days of missing data.

SPZs are largely reflected in the intraseasonal variations of the SPZs. The relationships of the intraseasonal variations of the SPZs to the monsoon convection (*e.g.*, Murakami, 1984), and to the midlatitude circulation (*e.g.*, Streten and Zillman, 1984) have been reported. Although the mechanisms of the intraseasonal variations of the SPZs are interesting to study, we will discuss the characteristics of the PSZs only in their active phases when they appear as clear cloud bands in the ten-day mean high-cloudiness fields.

4. Rainfall amount

As discussed in Section 1, the rainfall amount of the BFZ is comparable to that of the ITCZ. Yoshino (1966) investigated the climatic rainfall amount of the BFZ. According to Fig. 1-9 of Yoshino (1966) on the seasonal march of climatic ten-day mean precipitation distributions, the rainfall amount of the BFZ attains a maximum of more than 100 mm/10 day between mid-June and early-July, when an expecially large rainfall amount of ~150 mm/10 day is observed over China and the southwestern part of Japan.

In this section, we will compare the rainfall amount of the SPZs, using two types of precipitation data, station data and satellite data, evaluated from the high-cloudiness by the method of Maruyama *et al.* (1986).

4.1 Station data

To compare the rainfall amounts of the BFZ and the SPCZ, we investigated the precipitation at Kagoshima (31°N, 130°E) and at Rapa (28°S, 144°W), where the BFZ and the SPCZ, respectively, are frequently observed during the summer. The locations of these stations are shown in Fig. 2 by black circles. Unfortunately, no observation stations are found at appropriate sites to discuss the rainfall amount of the SACZ.

Figure 5 shows daily variations of precipitation at Kagoshima and Rapa during the FGGE year from December 1978 to November 1979. The sources of data are the Monthly Report of the JMA for Kagoshima and the FGGE level II-c precipitation and snow data set for Rapa.

At Kagoshima, both the rainfall amount and the number of days with precipitation increase and precipitation is apt to continue for several days during the northern early summer from June to July. These seasonal changes are observed almost every year and are associated with a seasonal stagnation of the Baiu front. The rainfall amount in June 1979 was ~400 mm, which is nearly as much as the climatic value at Kagoshima in June (400 mm) during the thirty years from 1961 to 1990.

At Rapa, the rainfall amount and the number of days with precipitation also increase during the southern summer. Monthly rainfall at Rapa is ~350

mm in January and ~700 mm in March, which is comparable to the climatic amount of the Baiu front.

Intraseasonal variations of precipitation are more significant at Rapa than at Kagoshima. This is due to the significant intraseasonal variations of the SPCZ shown in the last section; Fig. 3 shows that the rainfall amount at Rapa increased when the SPCZ was clearly observed around Rapa. Here we emphasize that the SPCZ has as much rainfall as the BFZ when the SPCZ is active.

The rainfall at Kagoshima and Rapa may be affected by topography, because the former lies ~10 km west of a 1100 m mountain and the latter lies ~5 km southeast of a 650 m mountain. We think, however, that the influence of topography is small enough to infer that the SPCZ provides nearly as much rainfall as the BFZ. The reasons for our inference are as follows: (1) There is a good correlation between the rainfall amount at Rapa and the positions of the SPCZ (Fig. 3), which suggests that the precipitation at Rapa is not localized and chiefly brought about by the strong convection in the SPCZ. (2) The climatic rainfall amount at Kagoshima during the early summer is not very different from that at the neighboring stations of Kagoshima (*cf.*, Yoshino, 1966).

4.2 Satellite data

The high-cloudiness derived from satellite imagery are useful for evaluating the rainfall amount over the ocean, free from the influence of topography. Maruyama *et al.* (1986) compared the monthly mean high-cloudiness derived from the Geostationary Meteorological Satellite (GMS) to the monthly mean rainfall amount observed over islands without high mountains over the western Pacific and the eastern Indian Ocean. They found a good correlation between the high-cloudiness and the rainfall amount both in the tropics and the summertime subtropics. They proposed an equation to evaluate the monthly amount of rainfall in the tropics between 20°N and 20°S from the monthly mean high-cloudiness, *i.e.*,

$$P = 113 * C - 10 \qquad (1)$$

where P and C denote monthly amount of rainfall (mm) and monthly mean high-cloudiness (/10), respectively.

Since Eq. (1) is derived for the tropics, some errors are unavoidable in estimating the rainfall in the subtropics. However, much of the rainfall during the summer seems to be carried by tall convective clouds both in the tropics and subtropics. We thus used Eq. (1) to estimate the monthly amount of rainfall of the SPZs.

Graphs of the narrow-bars in Fig. 6 indicate seasonal changes of the monthly high-cloudiness of the

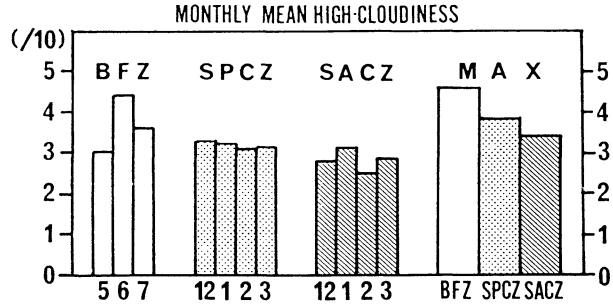

Fig. 6. Graphs of narrow bars show the seasonal change of monthly mean high-cloudiness of the BFZ along 130°E and of the SPCZ and the SACZ along 30°S. The high-cloudiness is averaged for the seven seasons of the N.H. early summer between May and July from 1979 to 1985 for the BFZ and of the S.H. summer between December and March from 1979/1980 to 1985/1986 for the SPCZ and the SACZ. Units are tenths of cloudiness. Graphs of wide bars show the maximum high-cloudiness of the SPZs, which is defined as the seven-year mean of the maximum of the monthly high-cloudiness of the SPZs for each season.

SPZs. Since the positions of the SPZs are variable, the cloudiness of the SPZs is defined as the maximum cloudiness along 130°E between 20°N and 40°N for the Baiu front, along 30°S between 120°W and 180° for the SPCZ, and along 30°S between 20°W and 40°W for the SPCZ and the SACZ. Furthermore, the cloudiness was averaged for seven seasons of the N.H. early summer between May and July from 1979 to 1985 for the BFZ and for seven seasons of the S.H. summer between December to March from 1979/1980 to 1985/1986 for the SPCZ and the SACZ.

For the BFZ, which climatically appears between May and July, the cloudiness clearly increases in June. For the SPCZ and the SACZ, on the other hand, such a distinct seasonal change is not found and monthly cloudiness during the summer is much less than the Baiu front in June.

We then selected the maximum of the monthly cloudiness of the SPZs for each summer and averaged it for the seven seasons of the analysis period. The averaged cloudiness is referred to as 'the mean maximum cloudiness' and shown by the histogram with wide-bars in Fig. 6.

The difference between the mean maximum cloudiness and the monthly cloudiness is large for the SPZs in the S.H. For the SPCZ, the mean maximum cloudiness is 3.8 and the maximum of the monthly cloudiness is 3.3 in December. For the SACZ, the former is 3.4 while the latter is 3.1 in Jan-

uary. However, the difference is small for the BFZ, *i.e.*, the mean maximum cloudiness is 4.6 and the maximum of the monthly cloudiness is 4.4 in June. Figure 6 implies that the month when the maximum cloudiness is observed is virtually confined to June for the BFZ and cannot be specified for the SPZs in the S.H.

Although the differences among the SPZs are interesting, we would like to note that the mean maximum cloudiness of the SPCZ and the SACZ is more than 3.3, which corresponds to a monthly rainfall of 360 mm according to Eq. (1). This amount is comparable to that of the BFZ, although the mean maximum cloudiness of the Baiu front is 4.6 and the estimated monthly rainfall of ~500 mm is rather larger than that of the SPZs in the S.H.

4.3 Remarks

According to previous studies, the climatological monthly amount of rainfall along the SPCZ and the SACZ is smaller than along the BFZ (*e.g.*, Jaeger, 1976). This seems partly because the month when the monthly rainfall becomes maximum is not specified for the SPZs in the S.H., because this makes the long-term mean rainfall amount of the SPZs small, although a large rainfall amount is observed when the SPZs are active. Furthermore, the SPCZ is apt to have a large shift in the zonal direction (not shown) and this shift also can decrease the rainfall observed at fixed stations.

For example, the climatological amount of monthly rainfall derived for thirty years from December 1960 to November 1990 is 400 mm at Kagoshima in June and 258 mm at Rapa in January. There is a large difference between them. The long-term mean of the maximum amount of monthly rainfall in each summer between December and March is 398 mm at Rapa, which is nearly the same as the climatological amount at Kagoshima in June. These amounts were calculated using the World Weather Record (1960–1970) and the Monthly Climatic Data for the World (1971–1990) for Rapa and the Monthly Report of the JMA for Kagoshima. When we calculated the mean of the maximum amount, three seasons of the S.H. summer (1974/1975, 1988/1989, and 1989/1990) were excluded because these seasons include months when the precipitation data were missing.

In conclusion, the monthly rainfall amount of the Baiu front and the SPCZ is ~400 mm when they are active. The monthly rainfall amount of the SACZ also seems to be comparable to that of the other two SPZs because only small differences of the high-cloudiness are found among them, although the rainfall amount of the SACZ should be confirmed by other data at some future time.

5. Large-scale characteristics

As discussed in Section 1, the BFZ has several unique characteristics different from both the PFZs and the ITCZ. Ninomiya (1984) proposed that the BFZ should be classified as a subtropical frontal zone. In this section, we will investigate the large-scale characteristics of the SPZs, especially their interior structure and surrounding circulation, and show that the SPCZ and the SACZ have several characteristics different from both the PFZs and the ITCZ, but similar to the BFZ.

The SPZs change their characteristics on various time scales. To clarify the large-scale features of the SPZs by filtering out synoptic and subsynoptic variations, we analyzed ten-day mean data. Furthermore, to filter out intraseasonal and interannual variations of the SPZs, we employed a composite technique. For this composite the ten-day mean data are averaged for the selected periods when each SPZ is active, referring to the positions of the SPZ determined by the ten-day mean high-cloudiness distributions.

The selection of the ten-day periods was done by examining whether each SPZ meets the following two criteria in the high-cloudiness fields; (1) the SPZ appears as a single clear cloud band, and (2) the maximum high-cloudiness along the SPZ between 30° and 35° latitude is more than 4/10. The numbers of the selected ten-day periods were 12, 14, and 12 for the BFZ, the SPCZ, and the SACZ, respectively. In most of the selected periods, the SPZs almost stagnated intermittently with large cloudiness on a daily bases (not shown).

The composites were done to overlay the reference points which indicate the positions of each SPZ during each selected period. Here, the reference points were defined as the points where the BFZ intersects the meridian of 130°E and the SPCZ and the SACZ intersect the parallel of 30°S. This is because the BFZ shifts meridionally rather than zonally and the SPZs in the S.H. shift zonally rather than meridionally. To overlay the reference points, the fields were moved in zonal and meridional directions without rotation, although there are slight directional changes in the axes of the SPZs. Table 1 shows the selected ten-day periods and reference points for the composite.

In the following discussions, only the composite fields will be shown to save space. Analyses were, however, done for all of the selected periods and the qualitative features shown in the composite figures were commonly observed in all the selected periods.

5.1 Wind fields

Figure 7 shows composite fields of the high-cloudiness around the SPZs. Coastlines, parallels, and meridians are shown to indicate the mean positions of the SPZ averaged for the selected ten-day

Table 1. Periods and reference points utilized for the composite analysis.

		1	2	3	4	5	6	7	8	9	10	11	12	13	14
Baiu front	Period: Y, M	1981, 6	1981, 6	1982, 6	1982, 6	1982, 7	1983, 6	1983, 6	1983, 7	1983, 7	1985, 6	1985, 6	1985, 7		
	Day	11-21	21–30	1–10	11–20	11–20	11–20	21–30	1–10	11-20	11–20	21–30	1–10		
	Ref. P.: Lat (°N)	35	35	30	30	32.5	30	30	30	35	32.5	35	35		
	Lon (°E)	130	130	130	130	130	130	130	130	130	130	130	130		
SPCZ	Period: Y, M	1981, 2	1981, 3	1981, 3	1981, 12	1982, 1	1983, 1	1983, 12	1983, 12	1985, 1	1985, 2	1985, 3	1985, 3	1985, 12	1985, 12
	Day	11–21	1–10	11–20	21–31	21–31	11–20	1–10	21–31	21–31	21–28	1–10	21–31	1–20	21–31
	Ref. P.: Lat (°S)	30	30	30	30	30	30	30	30	30	30	30	30	30	30
	Lon (°W)	142.5	132.5	140	140	160	117.5	140	130	140	157.5	150	180	147.5	130
SACZ	Period: Y, M	1981, 1	1982, 1	1982, 3	1982, 12	1983, 1	1983, 1	1983, 2	1983, 3	1983, 12	1985, 1	1985, 1	1985, 2		
	Day	11–21	1–10	1–10	1–10	1–10	11–20	21–28	1–10	11–20	1–10	11–20	21–28		
	Ref. P.: Lat (°S)	30	30	30	30	30	30	30	30	30	30	30	30		
	Lon (°W)	35	40	25	35	25	25	50	40	32.5	27.5	30	25		

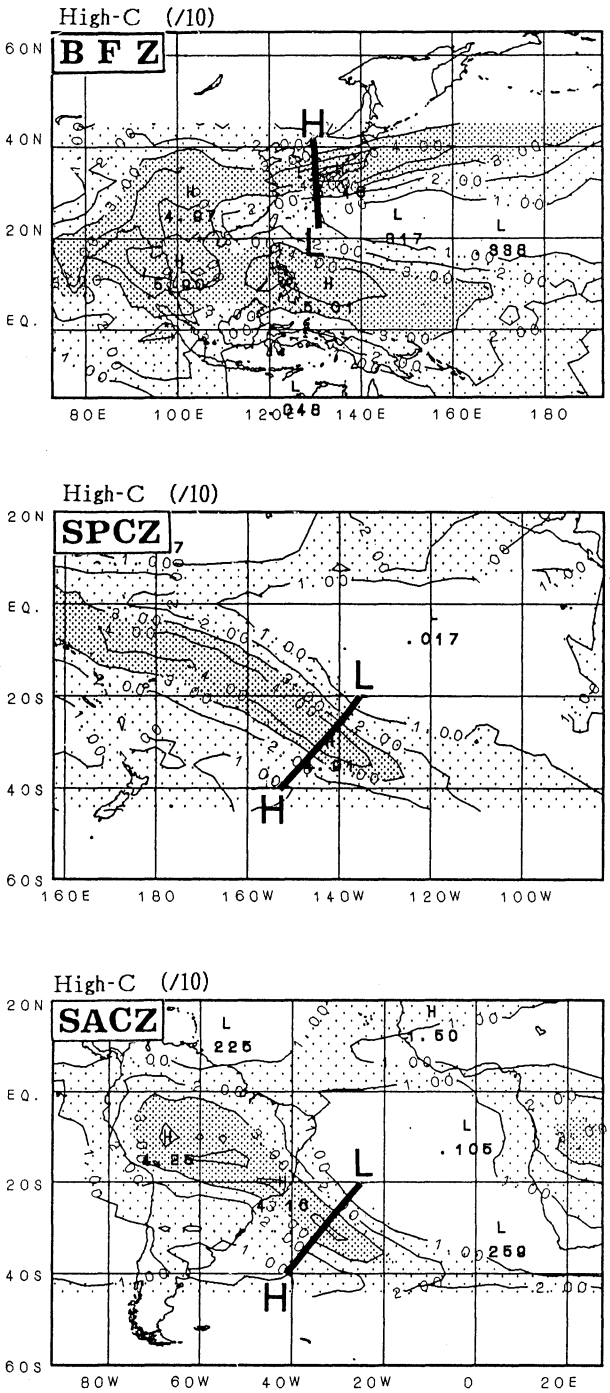

Fig. 7. Composite fields of the high-cloudiness around the SPZs. Contour interval is 1/10 and the areas of the high-cloudiness between 1/10 and 3/10 are thin shaded while more than 3/10 are thick shaded. The high-cloudiness is not shown north of 45°N are south of 45°S. Thick solid lines in the figures indicate the positions of cross-sections utilized in the present study.

periods. Thick lines indicate the positions of cross-sections utilized in the following discussions. As discussed in Section 3, all of the SPZs extend northeastward (in the N.H.) or southeastward (in the S.H.) from the monsoon convection in the tropics. A difference is found in the ITCZ equatorward of the SPZs; the ITCZ is more vigorous to the south of the BFZ than north of the SPCZ and the SACZ. This difference may be related to the moisture transport around the SPZs, which will be discussed in Part II.

Figure 8 shows composite fields of 300 mb geopotential height around the SPZs. Thick lines indicate the positions of the SPZs for the portions to be studied: around Japan between 120°E and 160°E for the BFZ and the subtropics between 25°S and 40°S for the SPCZ and SACZ.

Troughs of the subtropical jet penetrate into the subtropics at ~30°N or ~25°S and all of the SPZs extend along the subtropical jet in the eastern part of the troughs. The troughs commonly form to the northeast (in the N.H.) or to the southeast (in the S.H.) of upper highs observed in the tropics, which correspond to upper tropospheric divergence of the monsoon convection (Fig. 7). Possible relationships between the troughs and the monsoon convection will be discussed in Part II.

Figure 9 shows composite fields of wind and geopotential height at 1000 mb. Here, we can obtain height and wind fields not at 1000 mb but at the surface in 1985 from the JMA analysis. For 1985, we substituted surface wind for 1000 mb wind and calculated the 1000 mb height from surface pressure by assuming the hydrostatic approximation and a constant air temperature between the surface and 1000 mb equal to the surface air temperature.

Figure 9 clearly shows that all of the SPZs have a low-level inflow which appears along the northwestern (in the N.H.) or southwestern (in the S.H.) periphery of subtropical highs. In the previous studies of the BFZ, the low-level inflow along the periphery of the subtropical high has been mentioned, because it transports much moisture to the front (*e.g.*, Murakami, 1959; Akiyama, 1973) and generates convective instability with increasing equivalent potential temperature at low-levels (Ninomiya, 1978). Figure 9 indicates that similar inflows are observed for the SPZs in the S.H.

Figure 10 shows composite fields of wind in the cross sections of the SPZs. Positions of the sections were previously shown in Fig. 7. Solid contours indicate the wind speed component parallel to the SPZs and dashed contours indicate the wind speed component normal to the SPZs. Areas where the wind speed blowing into the SPZ from low latitudes is more than 2 m/s are shaded.

For each SPZ, the wind component parallel to the SPZ becomes stronger with height and forms the westerly jet in the upper troposphere. This feature is similar to that of PFZs and this similarity indicates that the SPZs are characterized as baroclinic frontal zones.

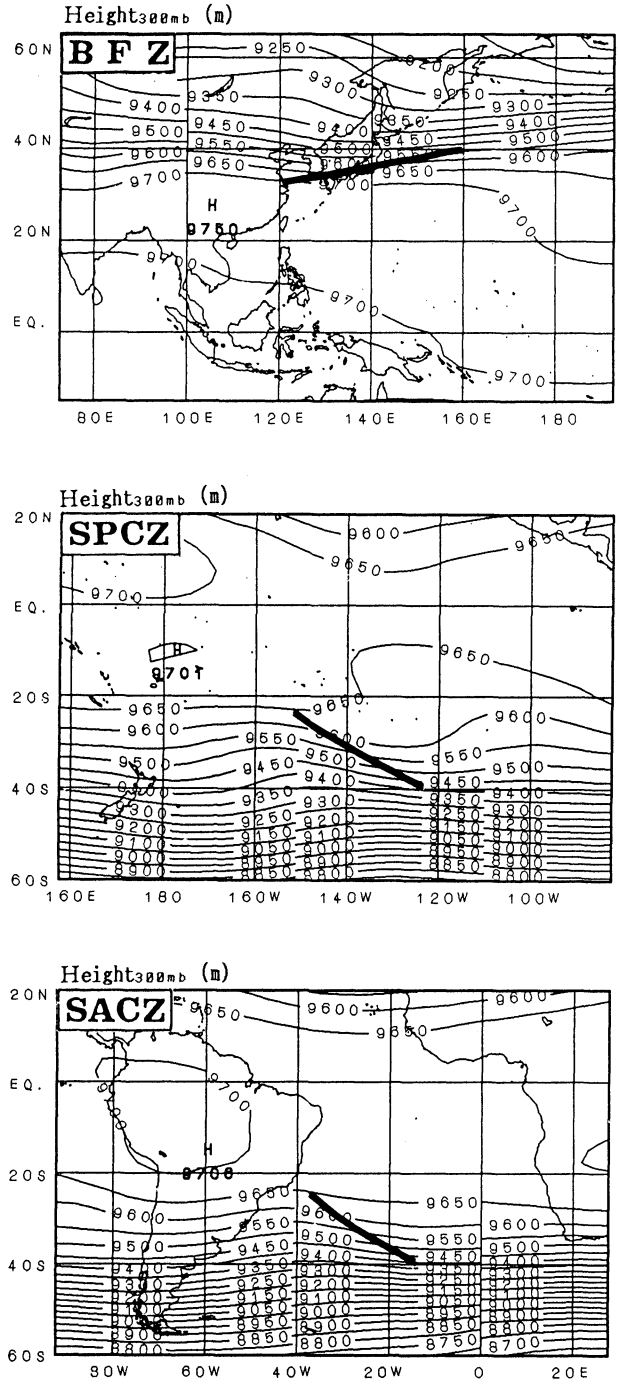

Fig. 8. Composite fields of 300 mb geopotential height around the SPZs. Contour interval is 50 m. Thick solid lines in the figures indicate the mean positions of the SPZs detrmined from the composite high-cloudiness fields shown in Fig. 7.

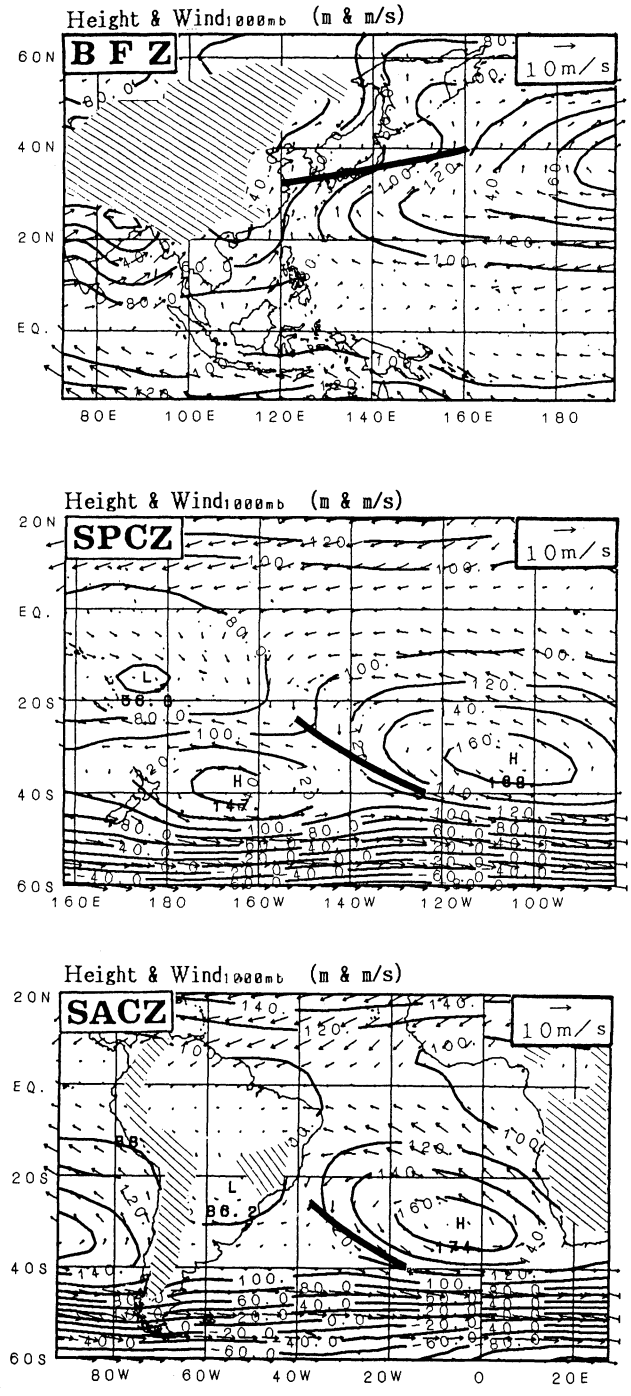

Fig. 9. As in Fig. 8 but for wind and geopotential height at 1000 mb. Contour interval is 20 m.

For the wind component normal to the SPZs, we can find the baroclinic wind structure; there are inflows from the low latitudes in the lower and middle troposphere and outflows to the low latitudes in the upper troposphere. The inflows correspond to the low-level inflows observed along the northwestern or southwestern periphery of the subtropical high shown in Fig. 9.

Figure 11 shows composite fields of horizontal wind divergence in the cross-sections of the SPZs. A linear correction of the horizontal divergence increasing with height is used to make $\omega = dp/dt$, which is obtained by the continuity equation, vanish

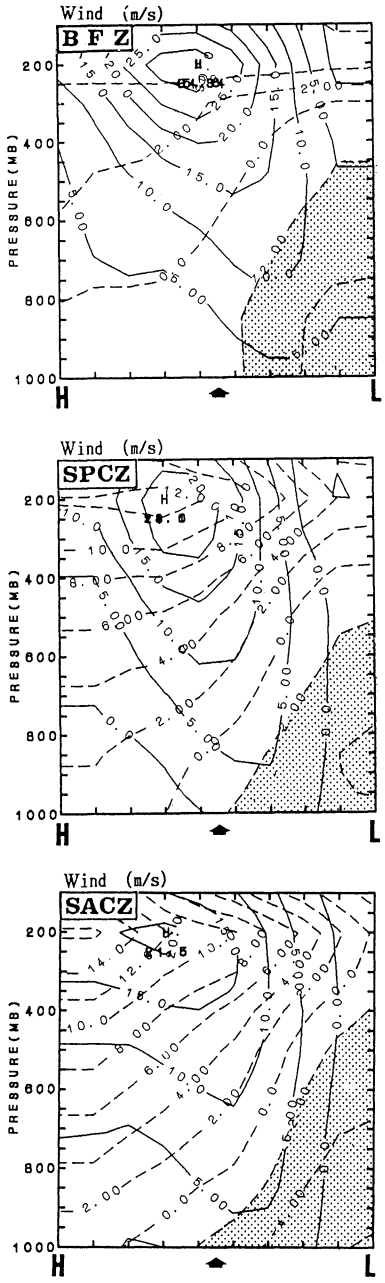

Fig. 10. Composite fields of wind speed in the cross-section of each SPZ. Solid and dashed contours indicate the speed of wind parallel to the SPZ and normal to the SPZ, respectively. Interval of the solid contours is 5 m/s and positive speed indicates that the wind parallel to the SPZ has an eastward component. Interval of the dashed contours is 2 m/s and positive speed indicates that the wind normal to the SPZ has a poleward component. The areas where the wind normal to the SPZ is more than 2 m/s in the equatorward side of each SPZ are shaded. An arrow and characters of 'L' and 'H' at the bottom of each panel indicate the positions of the center of each SPZ and of the two ends of the cross-section shown in Fig. 7, respectively.

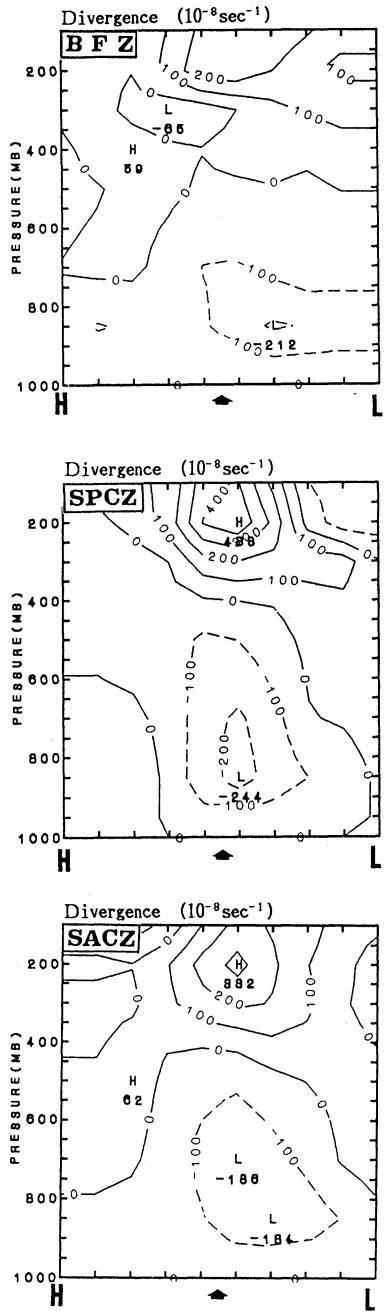

Fig. 11. As in Fig. 10 but for devergence of horizontal wind. Contour interval is 100 $\times 10^{-8}$/s.

at 100 mb. Every SPZ has convergence in the lower and middle troposphere and divergence in the upper troposphere. Although the maximum of the low-level convergence is $\sim 2 \times 10^{-6}$/s and less than that of the ITCZ $\sim 5 \times 10^{-6}$/s (*e.g.*, Reeves *et al.*, 1979), Fig. 11 shows that all of the SPZs are characterized by convergence zones.

Figure 12 shows composite fields of standard deviations of vorticity at 500 mb. Here, the standard deviations were calculated for every selected ten-day period using daily 500 mb wind fields and then were

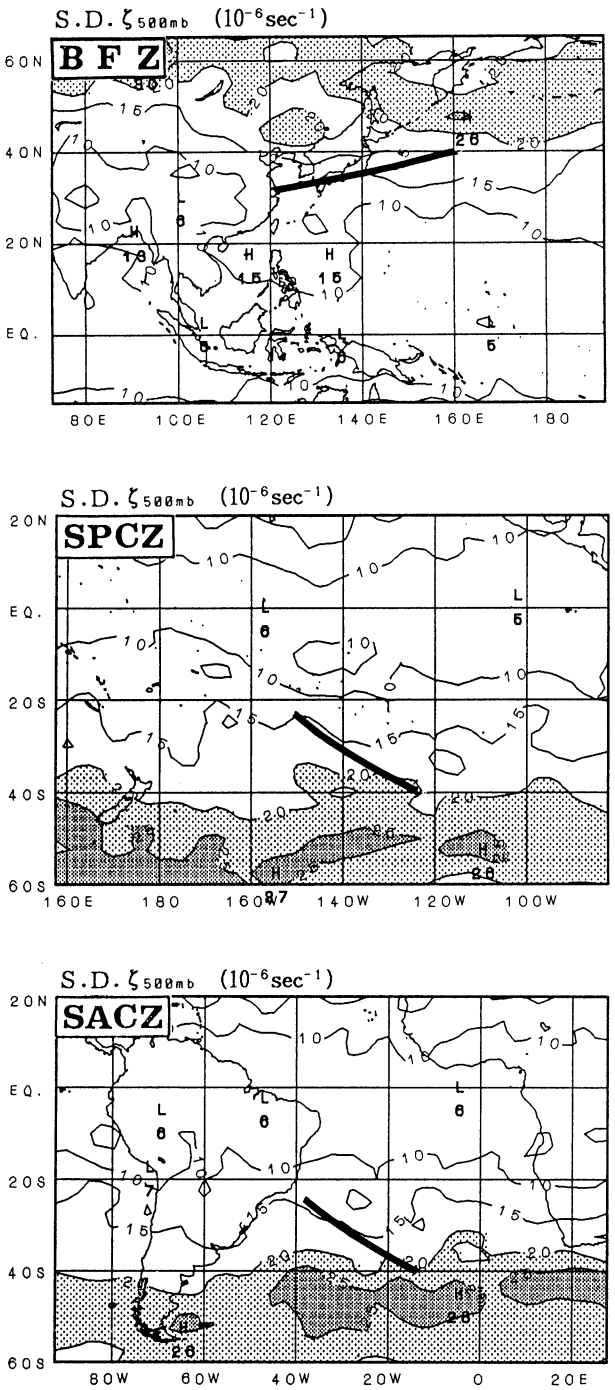

Fig. 12. As in Fig. 8 but for standard deviations of vorticity at 500 mb, which are calculated from daily wind data. The contour interval is 5 m; the areas of variation between 20×10^{-7}-25×10^{-7} are thin shaded and more than 25×10^{-7} are thick shaded.

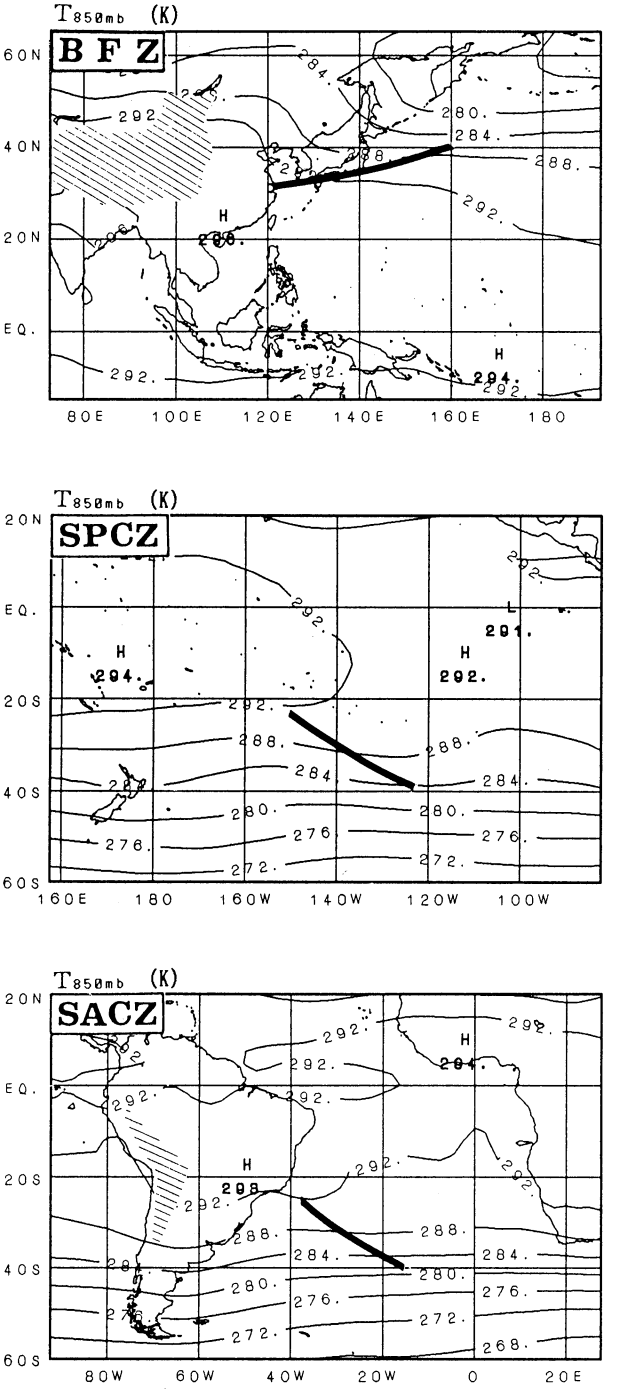

Fig. 13. As in Fig. 8 but for temperature at 850 mb. Contour interval is 4K.

composited. Polar frontal zones around 50°N and 50°S are characterized by a large vorticity variation. The vorticity variation along the SPZs is much smaller, and the SPZs are characterized by their steadiness.

5.2 Temperature and moisture fields

Figure 13 shows composite fields of temperature at 850 mb. All of the SPZs are associated with a rather large temperature gradient. Figure 14 shows composite fields of temperature anomalies in the cross-sections of the SPZs. Here, the temperature anomalies are defined as deviations from the mean temperature averaged over the cross-section for each pressure level. All of the SPZs are associated with

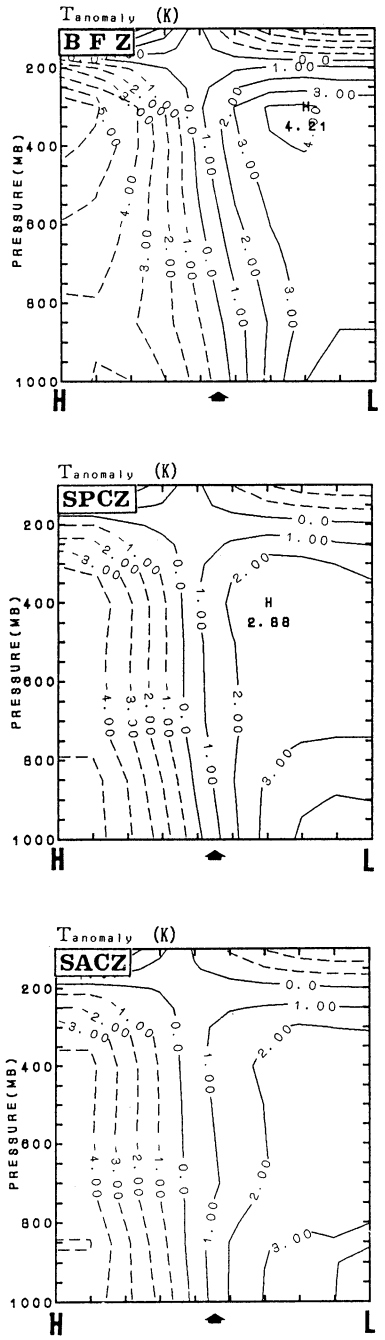

Fig. 14. As in Fig. 10 but for temperature anomaly from the mean temperature averaged for each pressure level along the cross-section. The contour interval is 1K.

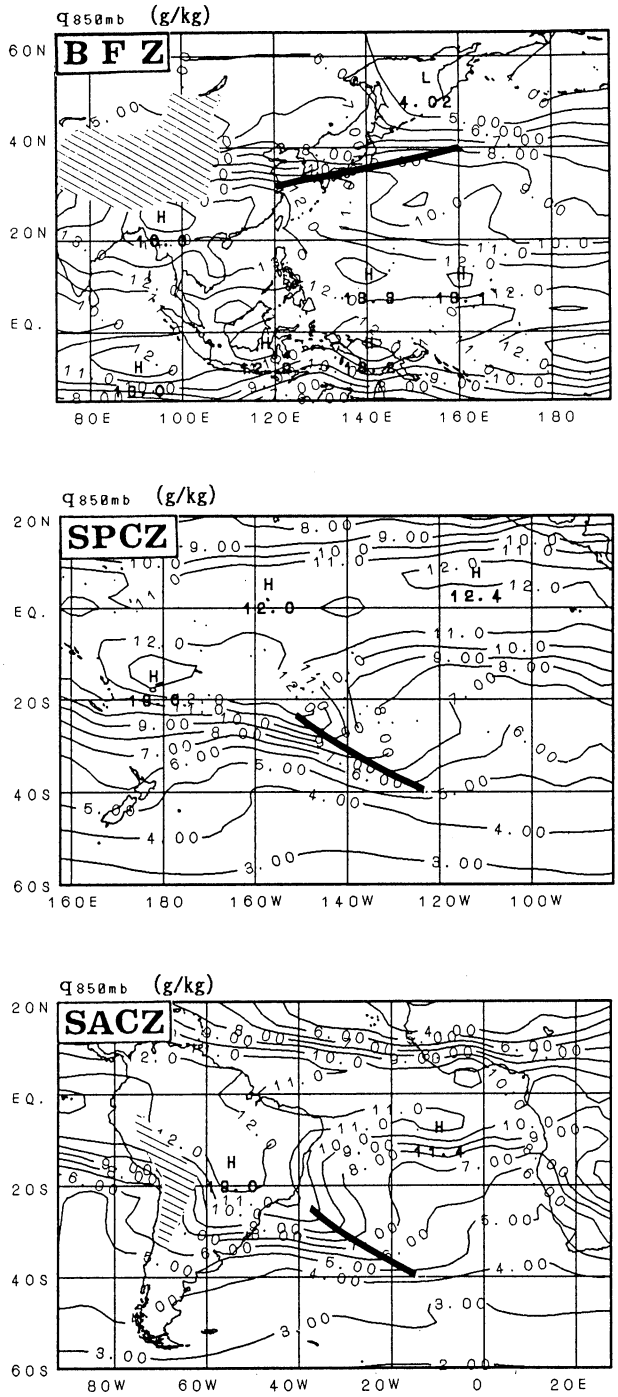

Fig. 15. As in Fig. 8 but for moisture mixing ratio at the 850 mb level. The contour interval is 1 g/Kg.

baroclinicity as shown by a fairly large temperature gradient around 5K/1000 km.

Ninomiya (1984) stressed that the low-level temperature gradient is weaker in the BFZ than in the PFZs. Certainly, low-level baroclinicity of the BFZ is very weak over and around the China continent. The baroclinicity of the BFZ, however, increases with distance from the continent. Although the low-level temperature gradient of the BFZ over the ocean and the SPZs in the S.H. may be somewhat smaller than that of the PFZs (Fig. 13), it should be stressed that the SPZs are associated with a fairly large temperature gradient, unlike the ITCZ. This is because the baroclinicity may strongly affect the characteristics of the precipitation systems developed in the SPZs.

Figure 15 shows composite fields of the mixing-ratio at 850 mb around the SPZs. All of the SPZs

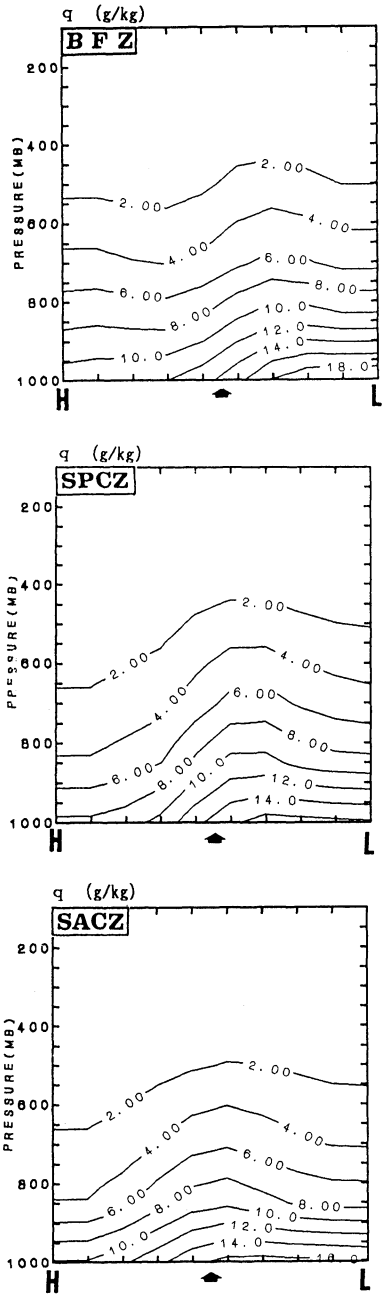

Fig. 16. As in Fig. 10 but for moisture mixing ratio. The contour interval is 2 g/Kg.

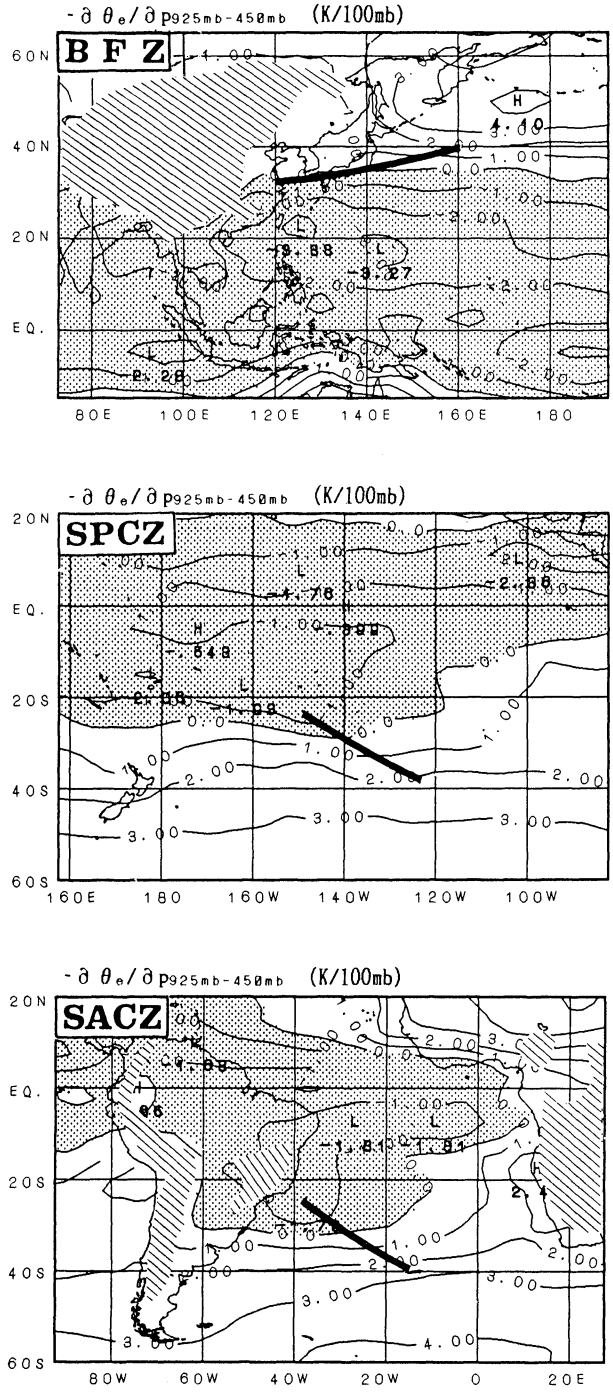

Fig. 17. As in Fig. 8 but for $-\frac{\partial \theta_e}{\partial p}$ in the 925–450 mb layer. The contour interval is 1K/100 mb.

are associated with a large gradient of mixing-ratio along their poleward side. Such a large gradient is not found for the PFZs at ~50°N or ~50°S. The BFZ forms the poleward boundary of the moist tropical or monsoon airmass (Saito, 1966; Akiyama, 1973). Figure 15 indicates the SPZs in the S.H. also form poleward boundaries of the moist airmass.

Figure 16 shows composite fields of the moisture mixing-ratio in the cross-section of the SPZs. All of the SPZs are associated with interior thick moist layers, which suggest upward moisture transport in the SPZs, and a low-level large gradient of mixing ratio at their poleward side.

5.3 Stratification

Figure 17 shows composite fields of $-\frac{\partial \theta_e}{\partial p}$ between 925 mb and 450 mb. For all of the SPZs, $-\frac{\partial \theta_e}{\partial p}$ is -1 ~$+2$K/100 mb and stability along the SPZs is moist neutral. All of the SPZs are located between a convectively unstable airmass in the low latitudes and a stable airmass in the mid latitudes. Polar frontal zones are located in the stable airmass. These fea-

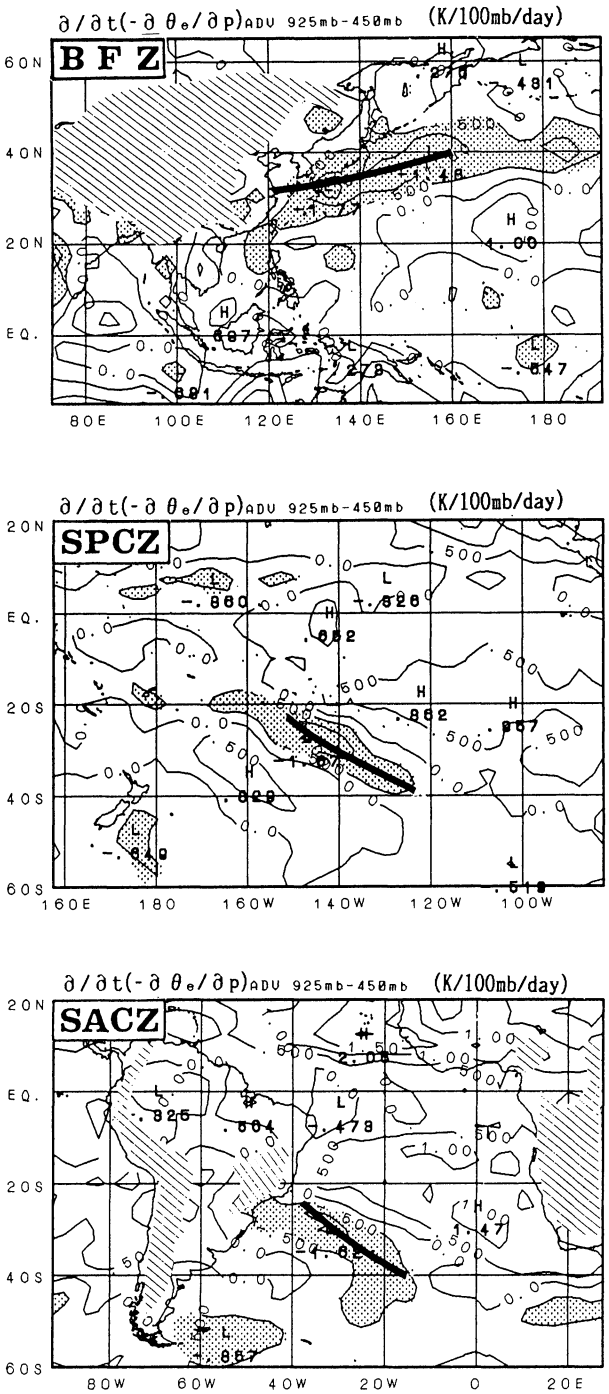

Fig. 18. As in Fig. 8 but for $\frac{\partial}{\partial t}(-\frac{\partial \theta_e}{\partial p})_{ADV}$ in the 925–450 mb layer. The contour interval is 0.5K/100 mb/day.

tures agree with the previous indication for the BFZ suggested by Ninomiya (1984).

Figure 18 shows composite fields of $\frac{\partial}{\partial t}(-\frac{\partial \theta_e}{\partial p})_{ADV}$ between 925mb and 450 mb, which indicate the temporal change of convective instability by the advective process. Here $\frac{\partial}{\partial t}(-\frac{\partial \theta_e}{\partial p})_{ADV}$ is expressed by

$$\frac{\partial}{\partial t}\left(-\frac{\partial \theta_e}{\partial p}\right)_{ADV} = \frac{\partial}{\partial p}\left(\bar{\boldsymbol{V}}\nabla\bar{\theta}_e + \bar{\omega}\frac{\partial \bar{\theta}_e}{\partial p}\right) \qquad (2)$$

where $(-)$ denotes the average for each selected ten-day period.

Ninomiya (1984) showed a steady generation of convective instability by the advective process along the BFZ, which provides a necessary condition for developing the convective clouds in the zone. Figure 18 indicates that all of the SPZs are characterized by the steady generation of strong convective instability. A similar generation of instability is not found in the PFZs.

Figure 19 shows $(\frac{\partial \theta_e}{\partial t})_{ADV}$ at 925 mb. Large $(\frac{\partial \theta_e}{\partial t})_{ADV}$ is found only along the SPZs. The moist low-level flow along the SPZs largely contributes to generating convective instability by increasing low-level potential temperature in the SPZs (not shown).[2]

The intensification of instability seems to be eliminated by the active convection in the SPZs and the most neutral stratification is preserved in the SPZs (Fig. 17).

5.4 Moisture supply

Along the BFZ, the rainfall rate is much larger than the evaporation rate and the convergence of moisture fluxes along the BFZ is important to maintain the large rainfall of the BFZ. Akiyama (1973) evaluated the monthly-mean evaporation rate along the BFZ to be less than 3 mm/day, which is much smaller than the mean precipitation rate of ~10 mm/day along it.

Previous studies pointed out there are two distinct moisture flow which converge along the BFZ. One is WSW flow along the front and the other is SW flow along the northwestern periphery of the Pacific subtropical high (*e.g.*, Murakami, 1959).

Figure 20 shows composite fields of SST and evaporation rate around the SPZs. The evaporation rate was estimated by the bulk method of Kondo (1975) using the daily surface objective analysis and climatic ten-day mean SSTs which were linearly interpolated from monthly climatic SSTs compiled by the Marine Department of JMA (1989). Selected ten-day periods for the composite analysis are the same as shown in Table 1 but only in 1985, because only the JMA data for 1985 include surface analysis necessary to estimate the evaporation rate. The positions of the SPZs shown in Fig. 20 are different from those in other figures, because we determined the positions using the high-cloudiness fields only in 1985.

The SST along the SPZs is much lower than along the ITCZ and positions of the SPZs disagree with

[2]Although the low-level moist flow along the western periphery of the subtropical high does not largely contribute to generating the convective instability in the composite fields, it may be large in some areas in snapshotted fields. Ninomiya (1978) reported a case when destablization on heavy rainfall area in the Baiu front was caused by this low-level flow.

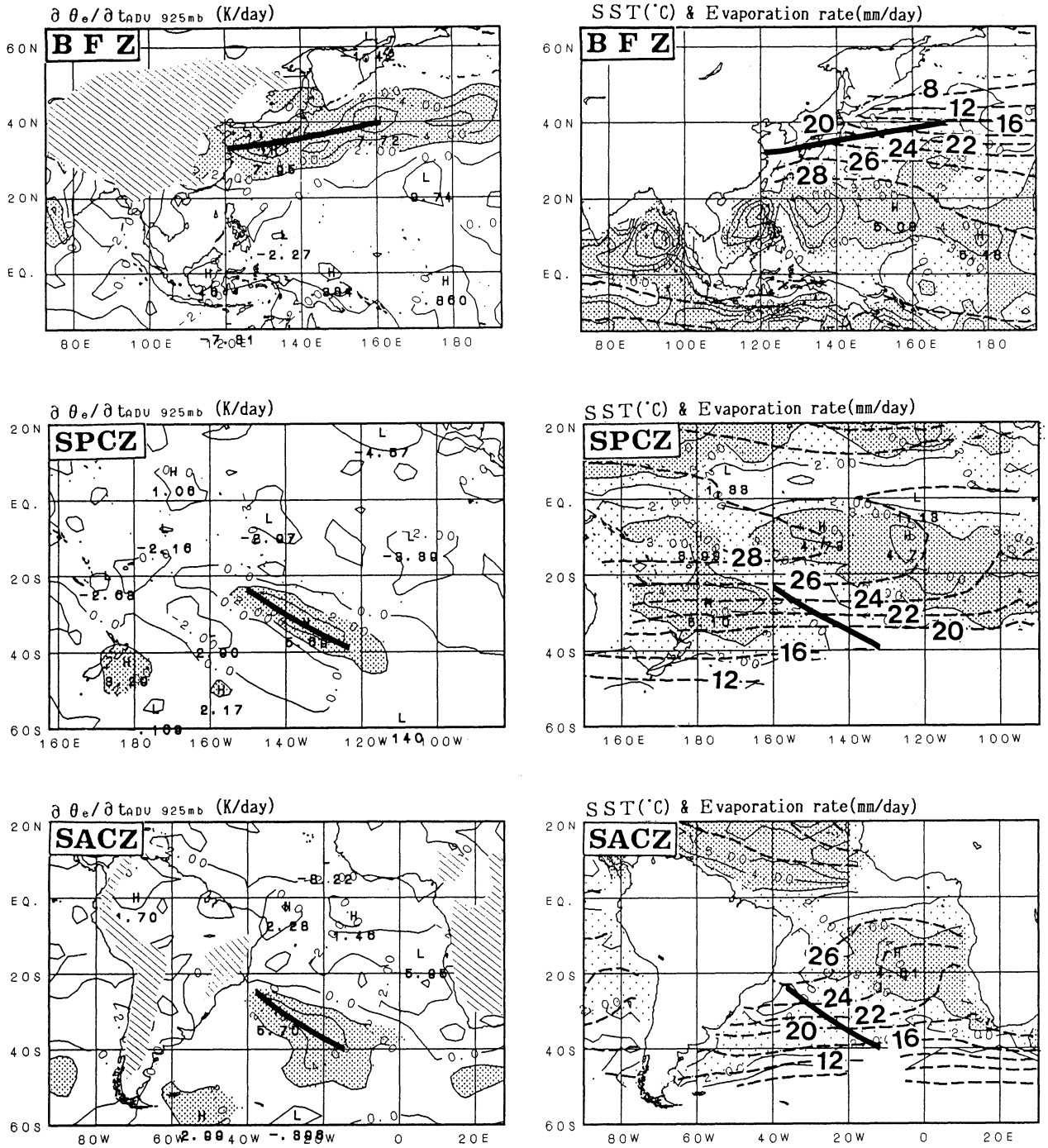

Fig. 19. As in Fig. 8 but for $(\frac{\partial \theta_e}{\partial t})_{ADV}$ at the 925 mb level. The contour interval is 2K/day.

Fig. 20. As in Fig. 8 but for evaporation rate and SST composited only for 1985. Solid contours indicate the evaporation rate at intervals of 1 mm/day. Dashed contours indicate the SST (°C) at intervals of 2°C. Thick and thin shade indicate the evaporation rates of more than 3 mm/day and between 1 mm/day and 3 mm/day, respectively. Positions of the SPZs shown by thick lines are slightly different from that in other figures because the positions are determined by the composite high cloudiness fields in 1985.

local SST maxima (*e.g.*, Kiladis *et al.*, 1989). The evaporation rate along the SPZs ~30°N and ~30°S is ~2 mm/day, which is much smaller than the precipitation rate of the SPZs of 10 mm/day. The small evaporation rate is mainly due to rather low SSTs of 22°C~26°C at ~30°N or ~30°S and a large relative humidity along the SPZs. Figure 20 also shows a relatively large evaporation rate of ~4 mm/day equatorward of the SPZs. The large rate is observed over

the subtropical highs (*cf.*, Fig. 9) and the moisture flow passing through these areas seems to be one of the main moisture sources of the SPZs, as shown in the following.

Reliability of the estimated evaporation rate may largely depend on the accuracy of the objective analysis data utilized. The author thinks that the reliability is fairly good because the estimated evaporation rates in the subtropical high nearly agree with climatological amounts of 3~5 mm/day determined by Hsiung (1986) using ship observation data for the 31 years from 1949 to 1979. Although the small evaporation rates along the SPZs shown in Fig. 20 are not clearly found in the maps of Hsiung (1986), the disagreement is probably due to the coarse resolution of Hsiung's maps of 5° latitude and 5° longitude.

The large difference between the rates of precipitation and evaporation along the SPZs should be compensated by the convergence of moisture fluxes. Figure 21 shows composite fields of the moisture fluxes integrated between 1000 mb and 400 mb together with their convergence represented by thick shading (more than 10 mm/day) and thin shading (more than 5 mm/day). Here we assumed that the surface moisture fluxes are equal to the fluxes at 1000 mb in 1985, because the JMA data for 1985 include the surface analysis and not the 1000 mb analysis.

All of the SPZs are associated with two types of moisture flows; one flows along the SPZs and the other flows toward the SPZs along the northwestern or southwestern peripheries of the subtropical high passing over the sea with a large evaporation rate shown previously in Fig. 20. All of the SPZs are characterized as convergence zones of these two flows. These features agree with the previous discussion of the BFZ. Though fields of moisture fluxes around the SPZs show significant intraseasonal variations (not shown), the two moisture flows are commonly observed in all of the selected ten-day periods.

The moisture flux convergence along the SPZ is 5–10 mm/day and nearly equal to the difference between the rates of precipitation and evaporation. This agreement indicates that convergence of the two flows is important to maintain the large rainfall of the SPZs.

The two types of moisture flows are generated by the two types of low-level wind shown in Fig. 10; one is along the SPZs and increases with height, and the other is along the north-western or south-western periphery of the subtropical high and decreases with height. The author believes that the monsoon convections are closely related to the formation of these two flows and this relationship will be discussed in Part II.

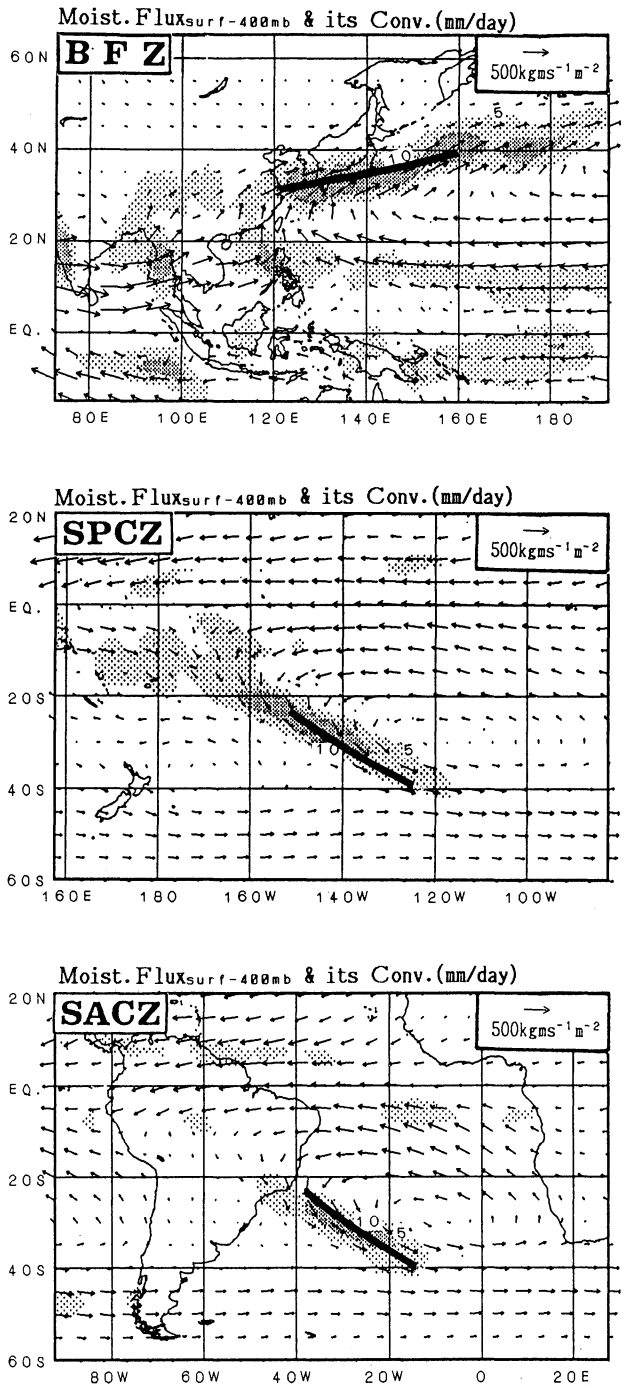

Fig. 21. As in Fig. 8 but for moisture flux intergrated between 1000 mb and 400 mb. Thick and thin shadings indicate the precipitation rates, which are determined by convergence of the moisture flux, more than 10 mm/day and more than 5 mm/day, respectively.

5.5 Remarks

As shown above, we found several large-scale characteristics of the SPZs in the S.H., which are similar to the unique characteristics of the BFZ. Ninomiya (1984) proposed that the BFZ is the sole subtropical

frontal zone in the N.H. during the summer. From the results of this section, we propose that the subtropical portions of the SPCZ and the SACZ should be classified as subtropical fronts.

In this section, the differences between the SPZs and the PFZs were discussed using composite fields. One may wonder whether the composite analysis is adequate to discuss the differences between the two zones, because the composite analysis referred to the SPZs' positions emphasizes the characteristics only of the SPZs and not of the PFZs. However, the differences between the two zones shown in the composite fields are not artificial, because the differences are more apparent in the ten-day mean fields in each selected period than in the composite fields (not shown).

Here, we should comment on the reliability of the objective analysis data utilized. Over the ocean, where aerological observation stations are sparse, the quality of the data seems to depend on the general circulationmodels used for the objective analysis. As discussed in Section 2, however, satellite data of cloud-winds and temperature soundings are utilized for the analysis over the ocean. Thus, the wind and temperature fields seem to be rather reliable, and it is trustworthy that every SPZ is characterized as both a baroclinic zone and a convergence zone, because this can be explained by using wind and temperature data.

The reliability of moisture fields over the ocean may not be very high and largely depend on the models utilized. The author has the impression that the low-level moisture gradient across the SPZs is somewhat larger in the NMC data that in the JMA data, although the low-level moisture gradient of the SPZs (*cf.*, Fig. 15) is clearly observed in both datasets. A quantitative analysis of the moisture fields, especially the moisture flux divergence (*cf.*, Fig. 21), should be re-examined in future.

6. Summary and Discussions

In the present study, we investigated the large-scale characteristics of the significant precipitation zones in the subtropics and found several common characteristics. The main findings are summarized as follows.

(1) In the subtropics during the summer, there are three significant precipitation zones: the Baiu frontal zone over East Asia and the western North Pacific, the SPCZ over the central South Pacific, and the SACZ over the South Atlantic. We called these zones the Subtropical Precipitation Zones (the SPZs). Although intraseasonal variations of the SPZs are significant, the rainfall amount of the SPZs is ~400 mm/month when they are active. Other weak precipitation zones in the subtropics appear to the east of North America and of Africa in the summer S.H.

(2) All of the SPZs extend eastward to the subtropics from localized monsoon convection in the tropics, while their surrounding land-sea distribution and topography have various differences among them. In the subtropics, the SPZs form along the upper subtropical jet in the eastern part of the troughs penetrating into the subtropics to ~25°S and ~30°N.

(3) The SPZs are characterized as convergence zones with interior thick moist layers and baroclinic zones with an upper subtropical jet. They are also characterized as poleward boundaries of moist tropical or monsoon airmasses associated with a large low-level moisture gradient, and by steady generation of convective instability by the differential advection process. This generation is important to preserve active convection in the SPZs, while stratification along the SPZs is moist neutral because of active convection.

Since the SPZs have several unique large-scale features different from PFZs and the ITCZ, they should be classified as subtropical frontal zones as proposed by Ninomiya (1984) for the BFZ.

(4) The SST along the SPZs is much lower than in the tropics, and the evaporation rate over the ocean along the SPZs is much smaller than the precipitation rate of the SPZs. Moisture transport by large-scale low-level winds is important to maintain the large rainfall of the SPZs. There are two major moisture flows converging along the SPZs; one flows along the northwestern (in the N.H.) or southwestern (in the S.H.) periphery of the subtropical high, invading into the SPZs from lower latitudes, and the other flows eastward along the SPZs.

In the present study, we found several common large-scale characteristics among the SPZs, although the topographic conditions surrounding them are very different. In the studies on the formation of the BFZ, the importance of the Tibetan Plateau, the Asian summer monsoon, and the subtropical high over the western North Pacific have been mentioned. The present study indicates that all of the SPZs have similar relationships to the tropical monsoon convection and subtropical highs. These findings strongly suggest the importance of the monsoon and subtropical high in forming the SPZs. In Part II, we will discuss the relationship among the SPZs, monsoon, and subtropical high in detail.

In this paper, we discussed only the common features of the SPZs and differences among the SPZs are yet to be studied. The differences should be investigated, because they may provide useful suggestions on the influence of the surrounding topography and land-sea distribution on the characteristics of the SPZs.

Furthermore, we found several unique large-scale features characterizing the SPZs as subtropical frontal zones. The reason why such unique frontal zones form in specific areas are interesting. To

clarify the reasons, it may be useful to investigate whether all fronts invading into the subtropics have characteristics similar to the SPZs using daily weather maps.

In the BFZ, unique meso-scale precipitation systems different from those in the ITCZ and PFZs appear (*e.g.*, Akiyama, 1978). Obviously, the large-scale characteristics of the BFZ as a subtropical frontal zone cause suchunique meso-system. Thus we can imagine that similar meso-scale precipitation systems may appear along the SPCZ and the SACZ.

As shown in Section 1, Vincent (1985) reported meso-α-scale frontal depressions in the SPCZ. However, our knowledge of the meso-systems in the SPZs in the S.H. is insufficient, mainly because they appear over the ocean where observation stations are sparse. In the near future, satellite data will make it possible to investigate the oceanic meso-systems in detail. The comparison of meso-systems in the SPZs may greatly contribute to understanding the mechanisms of precipitation systems in the subtropics.

Acknowledgments

The author would like to express his sincere thanks to Prof. T. Asai of Ocean Research Institute, University of Tokyo for his cheerful guidance and encouragement throughout this study. He also thanks Dr. K. Kato of Water Research Institute, Nagoya University, for his fruitful discussions on the Baiu front, Dr. J. Matsumoto, Univ. of Tokyo, for kindly reviewing the original manuscript and supplying the precipitation data of FGGE level-IIc, and Dr. K. Masuda, Univ. of Tokyo for kindly supplying the NMC data he compiled. Thanks are also extended to Dr. R. Kimura and Dr. K. Nakamura of ORI, Univ. of Tokyo, Prof. T. Matsuno, Center of Climate System Research, Univ. of Tokyo, Dr. Y. Nikaido of the Meteorological Research Institute, Japan Meteorological Agency, Dr. M. Hinokio of JMA, and Dr. K. Rikiishi of Hirosaki Univ., for fruitful discussions and encouragement. Thanks are also due to the Long-Range Forecast Division and the Numerical Prediction Division of JMA for providing the OLR data and the global analysis data of JMA, respectively. The author is also grateful to Dr.K.Ninomiya of JMA and two anonymous reviewers for providing valuable comments. NCARG was used to draw many figures in this paper. Part of this study was conducted when the author studied at ORI, Univ. of Tokyo. This study was partly supported by a Grant-in-Aid for Scientific Research by the Ministry of Education, Science, and Culture, Project No. 01740234.

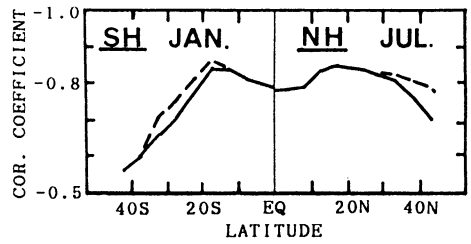

Fig. A1. Meridional variation of the correlation coefficient between the high-cloudiness and OLR in July in the Northern Hemisphere and in January in the Southern Hemisphere, determined for the area of East Asia and the western Pacific between 45°N and 45°S and between 90°E and 170°W and for the period from 1983 to 1985. The solid line is determined for the whole analyzed area and the dashed line is for the area excluding the Asian and Australian continents.

Appendix

OLR data have been utilized in tropical meteorology as a good indicator of convective activity. Since the OLR is influenced by not only cloudiness but air and surface temperature, OLR fields do not directly indicate cloudiness fields in the subtropics where seasonal and meridional temperature variation is large. We thus transformed the OLR to the high-cloudiness, which is defined as the amount of cloud with tops higher than the 400 mb level, by using statistical relationships between the OLR and the high-cloudiness to avoid the effects of temperature variation. The high-cloudiness is useful for investigating the rainfall activity of the SPZs, because the high-cloudiness correlates to the rainfall amount in the subtropics during the summer (Maruyama *et al.*, 1986).

The correlation coefficient between the high-cloudiness derived from GMS-IR observations and the OLR was calculated by using daily data for the area between 50°S and 50°N and between 90°E and 170°W during the three years from June 1982 to June 1985, except June 1984 because of a malfunction of the GMS. The calculation was done for every month and every zone of 5° width.

Figure A1 shows meridional variations of the correlation coefficient in January and July. Solid lines are for the entire area and dashed lines are for the area without the Asian and Australian continents. Although the absolute correlation coefficient decreases with increasing latitude, the absolute coefficients are more than 0.7 at ~30°N and more than 0.6 at ~30°S in the subtropics during the summer. These large absolute coefficients enable us to estimate the high-cloudiness from the OLR by linear

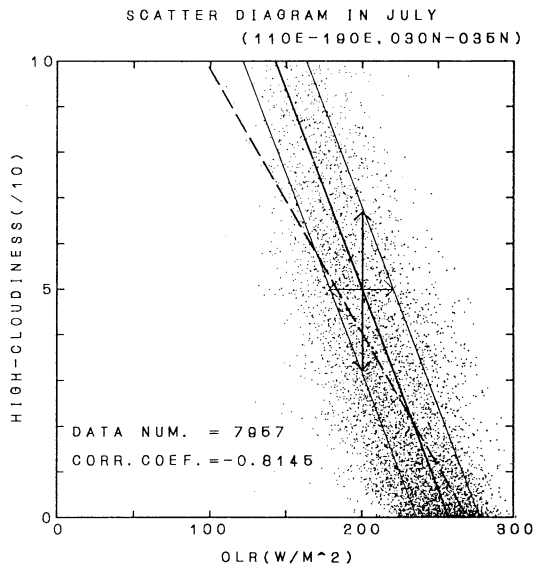

Fig. A2. A scatter diagram between the high-cloudiness and OLR for the area between 30°N and 35°N and between 110°E and 170°W in July between 1983 and 1985. The thick solid line is the regression line of OLR on the high-cloudiness and the dashed line is the regression line of the high-cloudiness on OLR. Two thin solid lines parallel to the thick line and thin arrows indicate one standard deviation of OLR from the regression line. Thick arrows indicate the magnitude of the standard error for estimating the high-cloudiness by using the regression line of OLR to the high-cloudiness.

regression for both the tropics and the summertime subtropics.

We then determined regression lines using the least squares method for every month and every zone of 5° width. To do this, we included the Australian continent and excluded the Asian continent because the correlation coefficient largely decreased when the Asian continent was included (*cf.*, Fig. A1).

Figure A2 shows an example of a scattering diagram of the OLR and the high-cloudiness. This figure also shows two types of regression lines; one is a line of the high-cloudiness on the OLR (dashed line) and the other is a line of the OLR on the high-cloudiness (thick solid line). Properly speaking, we should use the former to estimate the high-cloudiness from the OLR. However, the former is unnatural because the high-cloudiness varies on a step length confined between 0/10 and 10/10, and is concentrated around 0/10.

We thus used the regression line of the OLR on the high-cloudiness to estimate the high-cloudiness. Standard errors of the high-cloudiness are 1.2/10–2.1/10 between the equator and 40°N during the northern summer and 1.4/10–1.9/10 between the equator and 40°S during the southern summer. Here the standard error of the high-cloudiness was estimated from the standard error of the OLR in the way shown in Fig. A2. Thick and thin arrows in Fig. A2 indicate the standard errors of the high-cloudiness and the OLR, respectively.

References

Akiyama, T., 1973: The large-scale aspects of the characteristic features of the Baiu front. *Papers Met. Geophys.*, **24**, 175–188.

Akiyama, T., 1978: Mesoscale pulsation of convective rain in medium-scale disturbances developed in the Baiu Front. *J. Meteor. Soc. Japan*, **56**, 267–283.

Asakura,T., 1970: A study on climate variations around Japan and heat source/sink in the atmosphere. Part I: Tibetan Plateau and climate of Japan (in Japanese). *Meteorological Research Note*, **21**, 277–290.

Dey, C.H. and L.L. Morone, 1985: Evolution of the National Meteorological Center Global Data Assimilation System: January 1982–December 1983. *Mon. Wea. Rev.*, **113**, 304–318.

Huang, H.-J. and D.G. Vincent 1983: Changes in circulation features over the South Pacific during FGGE, 10–27 January 1979. *Mon. Wea. Rev.*, **111**, 1611–1618.

Hsiung, J., 1986: Mean surface energy fluxes over the global ocean. *J. Geophys. Res.*, **91**, 10585–10606.

Jaeger, L., 1976: Monthly precipitation for the whole world (in German). *Berichte des Deutschen Wetterdienstes*, **139**, 1–38.

Kanamitsu, M., K. Tada, T. Kudo, N. Sato and S. Isa, 1983: Description of the JMA operational spectral model. *J. Meteor. Soc. Japan*, **61**, 812–828.

Kato, K., 1985: On the abrupt change in the structure of the Baiu front over the China Continent in late May of 1979. *J. Meteor. Soc. Japan*, **63**, 20–36.

Kato, K., 1987: Airmass transformation over the semi-arid region around North China and abrupt change in the structure of the Baiu front in early summer. *J. Meteor. Soc. Japan*, **65**, 737–750.

Kato, K., 1989: Seasonal transition of the lower-level circulation systems around the Baiu front in China in 1979 and its relation to the Northern Summer Monsoon. *J. Meteor. Soc. Japan*, **67**, 249–265.

Kato, K. and Y. Kodama, 1992: Formation of the quasi-stationary Baiu front to the south of the Japan Islands in early May of 1979. *J. Meteor. Soc. Japan*, **70**, 631–647.

Kiladis, G.N., H. von Storch and H. van Loon, 1989: Origin of the South Pacific Convergence Zone. *J. Climate*, **2**, 1185–1195.

Kodama, Y. and T. Asai, 1988: Large-scale cloud distributions and their seasonal variations as derived from GMS-IR observations. *J. Meteor. Soc. Japan*, **66**, 87–101.

Kondo, J., 1975: Air-sea bulk transfer coefficients in diabatic conditions. *Boundary-Layer Meteor.*, **9**, 91–112.

Kurashima, A., 1959: General circulation and monsoon (in Japanese). *Kisetsufu (monsoon)*, Chijinshokan, 201–283.

Kurashima, A. and Y. Hiranuma, 1970: Is the Baiu front the polar front ? (in Japanese). *Tenki*, **17**, 245–246.

Marine Department, JMA., 1989: Climatic Charts of Sea Surface Temperature of the western North Pacific and the Global Ocean.

Maruyama, T., Ts. Nitta and Y. Tsuneoka, 1986: Estimation of monthly rainfall from satellite-observed cloud amount in the tropical Pacific. *J. Meteor. Soc. Japan*, **64**, 147–153.

McPherson, R.D., K.H. Bergman, R.E. Kistler, G.E. Rasch and D.S. Gordon, 1979: The NMC operational global data assimilation system. *Mon. Wea. Rev.*, **107**, 1445–1461.

Murakami, T., 1951: On the study of the change of the upper westerlies in the last stage of Baiu season (rainy season in Japan) (in Japanese with English abstract). *J. Meteor. Soc. Japan*, **29**, 162–175.

Murakami, T., 1956: The topographical effect upon the stationary upper flow patterns. *Pap. in Meteor. and Geophy.*, **7**, 69–89.

Murakami, T., 1959: The general circulation and Water-vapor balance over the Far East during the rainy season. *Geophys. Mag.*, **29**, 131–171.

Murakami, M., 1984: Analysis of the deep convective activity over the western Pacific and Southeast Asia. Part II: Seasonal and intraseasonal variations during Northern Summer. *J. Meteor. Soc. Japan*, **62**, 88–108.

Murakami, T., and T. Nakazawa, 1985: Transition from southern to northern hemisphere summer monsoon. *Mon. Wea. Rev.*, **113**, 1470–1486.

Murakami, T., 1986: Monsoon (in Japanese). Tokyo-do Press Co.

Nakamura, H. and N. Hasegawa, 1987: Forecast experiments on the large-scale features of the Baiu front. Short- and medium-range numerical weather prediction. *Sprecial Volume of J. Meteor. Soc. Japan*, 441–153.

Ninomiya, K., 1978: Heavy rainfalls associated with frontal depression in Asian subtropical humid region (I) Synoptic-scale features. *J. Meteor. Soc. Japan*, **56**, 253–266.

Ninomiya, K., 1984: Characteristics of Baiu front as a predominant subtropical front in the summer northern hemisphere. *J. Meteor. Soc. Japan*, **62**, 880–894.

Ninomiya, K. and H. Muraki, 1986: Large-scale circulations over East Asia during Baiu period of 1979. *J. Meteor. Soc. Japan*, **64**, 409–429.

Nitta, T., 1986: Long-term variations of cloud amount in the western Pacific region. *J. Meteor. Soc. Japan*, **64**, 373–390.

Ogawa, T., 1982: Rainfall phenomena over Polynesia (unpublished, in Japanese with English abstract). Bachelor thesis, Department of Geography, University of Tokyo.

Reeves, R.W., C.F. Ropelewski and M.D. Hudlow, 1979: Relationships between large-scale motion and convective precipitation during GATE. *Mon. Wea. Rev.*, **107**, 1154–1168.

Saito, N., 1966: A preliminary study of the summer monsoon of southern and eastern Asia. *J. Meteor. Soc. Japan*, **44**, 44–59.

Saito, N., 1985: Quasi-stationary waves in mid-latitudes and the Baiu in Japan. *J. Meteor. Soc. Japan*, **63**, 983–995.

Streten, N.A., 1973: Some characteristics of satellite-observed bands of persistent cloudiness over the Southern Hemisphere. *Mon. Wea. Rev.*, **101**, 486–495.

Streten, N.A. and J.W. Zillman, 1984: Climate of the South Pacific Ocean. *Climate of the Oceans (Van Loon, H., ed.)*, 263–371. World Survey of Climatology.

Taljarrd, J.J., 1967: Development, distribution and movement of cyclones and anticyclones in the Southern Hemisphere during the IGY. *J. Appl. Meteor.*, **6**, 973–987.

Taljarrd, J.J., 1968: Climatic frontal zones of the Southern Hemisphere. *Notes*, **17**, 23–34.

Trenberth, K.E., 1976: Spatial and temporal variations of the Southern Oscillation. *Quart. J. Roy. Meteor. Soc.*, **102**, 639–653.

Trewartha, G.T., 1968: An introduction of climate. McGraw-Hill Book Co.

Vincent, D.G., 1982: Circulation features over the South Pacific during 10–18 January 1979. *Mon. Wea. Rev.*, **110**, 981–993.

Vincent, D.G., 1985: Cyclone development in the South Pacific Convergence Zone during FGGE, 10–17 January 1979. *Quart. J. Roy. Meteor. Soc.*, **111**, 155–172.

Winston, J.S. and A.F. Krueger 1977: Diagnosis of the satellite-observed radiation heating in relation to the summer monsoon. *Pure. Appl. Geophys.*, **115**, 1131–1144.

Yasunari, T., 1977: Stationary waves in the Southern Hemisphere mid-latitude zone revealed from average brightness charts. *J. Meteor. Soc. Japan*, **55**, 274–285.

Yoshimura, M., 1967: Annual change in frontal zones in the Northern Hemisphere (in Japanese with English abstract). *Geograph. Rev. Japan (ser. A)*, **40**, 393–408.

Yoshino, M.M., 1966: Four stages of the rainy season in early summer over East Asia (Part II). *J. Meteor. Soc. Japan*, **44**, 209–217.

亜熱帯域の降水帯（梅雨前線帯、SPCZ、SACZ）にみられる大規模場の共通性 第1部：亜熱帯前線帯としての特徴

児玉安正
(弘前大学理学部地球科学科)

東アジアでは、初夏に梅雨前線帯と呼ばれる準定常的な前線帯があらわれ、ITCZに匹敵する多量の降水がもたらされる。梅雨前線帯は、ITCZや寒帯前線帯とは異なるいくつかの特徴を持ち、Ninomiya (1984)は梅雨前線帯は亜熱帯前線帯であるとした。本研究では、主として10日平均場の解析により夏季の南半球の顕著な降水帯であるSPCZ、SACZの亜熱帯域の部分を日本周辺域の梅雨前線帯と比較し、これら3つの降水帯が以下のような共通性を持つことを示す。

梅雨前線帯、SPCZ、SACZ（以下、亜熱帯降水帯）は、亜熱帯ジェットに沿って、熱帯モンスーンの降雨域の北東側（北半球）または南東側（南半球）に位置する準定常的なトラフの前面に形成される。亜熱帯降水帯の月降水量は、活動が活発なとき~400 mmに達する。すべての亜熱帯降水帯は、内部に厚い湿潤層を伴う収束帯としての性質と、上層の西風ジェットを伴う傾圧帯としての性質をあわせ持つ。さらに、湿潤な熱帯またはモンスーン気団の極側の外縁を成しており、下層の水蒸気傾度は大きい。

亜熱帯降水帯では、降水量が海面の蒸発量を大きく上回り、その降水の多くは、2種類の水蒸気流が降水帯で収束することにより維持される。その水蒸気流とは、降水帯に沿った東向きの流れと、亜熱帯高気圧の北西縁（北半球）または南東縁（南半球）に沿った流れである。後者は、亜熱帯高気圧の西部で蒸発した水蒸気を降水帯に輸送する。また、亜熱帯降水帯では下層で相当温位の高い空気の移流があり、これによる対流不安定の生成が降水帯の活発な対流活動を維持している。

SPCZとSACZは、梅雨前線帯と類似し、ITCZや寒帯前線帯とは異なる特徴を有しており、亜熱帯前線帯であると結論される。